

Latest Tortonian to early Pliocene interdune lake systems, southern Libya: Implications for the hydrology of the central Sahara

Mark W. Hounslow ^{a,b,*}, Helena E. White ^{c,e}, Nick Drake ^d, Vassil Karloukovski ^a, Sue J. McLaren ^e, Mustafa J. Salem ^f, Ahmed S. El-Hawat ^g, Osama Hlal ^f

^a Lancaster Environment Centre, Lancaster University, Lancaster LA1 4YW, UK

^b Earth, Ocean and Ecological Sciences, University of Liverpool, Jane Herdman Building, Liverpool L69 3GP, UK

^c University of Warwick, Kirby Corner Road, Coventry CV4 8UW, UK

^d Department of Geography, Kings College, London WC2R 2LS, UK

^e School of Geography, Geology and the Environment, University of Leicester, Leicester LE1 7RH, UK

^f Department of Geology, Faculty of Science, University of Tripoli, P.O. Box 13040, 13258 Tripoli, Libya

^g Earth Sciences Department, Faculty of Science, University of Benghazi, Benghazi, Libya



ARTICLE INFO

Editor: A Prendergast

Keywords:

Green Sahara
Magnetostratigraphy
Carbonate isotopes
Lacustrine dolomite
Hydrology
Hominin dispersal

ABSTRACT

Developing environmental and chronological data for the Miocene and Pliocene successions of the central Sahara provide a basis for refining the pacing of green Sahara episodes to consolidate debate about early hominin dispersal from eastern Africa. Sedimentological, isotopic and geomagnetic polarity datasets are used to assess the environment and age of the Zarzur Formation in eastern Fezzan, Libya. A magnetostratigraphy based on four sections, combined with a statistical comparison to the geomagnetic polarity timescale, indicate that the formation was deposited from 7.8 Ma to 4.3 Ma. Lacustrine facies comprise laminated, peloidal mud-grade carbonates (with localised gypsum) formed in varying fresh to hypersaline inter-dune lakes. A second lacustrine facies comprises gastropod- and ostracod-bearing calcareous sandstones, formed in lakes developed on sandy substrates. These systems evolved from earlier fluvial and sandy-playa environments developed in the latest Tortonian. Based on $\delta^{13}\text{C}$ and $\delta^{18}\text{O}$ from carbonates formed in the lacustrine systems and calcrite-related cements, water sources for the lake deposits varied between low to high salinity and were largely from westerly moisture sources likely from extreme precipitation events. Groundwater was an important source for the inter-dune lakes because of irregularity in precipitation. The timing of lacustrine carbonate formation was in part paced to deep lakes that developed in the East African Rift in the early Pliocene, although sandy substrate lakes also formed during the Messinian. Greening of the Libyan Fezzan during deposition of the Zarzur Formation promoted potential habitat pathways for early hominid dispersal from the Megalake Chad Basin.

1. Introduction

Our understanding of the timing, climate and environment of the Sahara in the Miocene and Pliocene is largely extrapolated from climate models (e.g. Zhang et al., 2014) and sediment cores from adjacent marine basins (Griffin, 1999; Larrasoña et al., 2013; Crocker et al., 2022; Amarathunga et al., 2024). This is partly due to the small number of preserved terrestrial sedimentary successions in the Sahara from this age interval, because the desert environment has largely eroded these sediments, but also the difficulty in precisely dating such terrestrial and lacustrine successions. Notwithstanding this, preserved sedimentary

deposits record numerous giant Saharan palaeolakes (Drake et al., 2022), a fact which has contributed to the debate about the nature of green Sahara episodes, and their link with hominin evolution and migration (Mirazon Lahr, 2010; Larrasoña et al., 2013; Maslin et al., 2014; Levin, 2015; Grine, 2016). Whilst there is a wealth of data about Late Quaternary to Holocene hominin-lacustrine associations in the central Sahara (Petit-Maire, 1991; Mattingley et al., 2003; Levin, 2015; Drake and Breeze, 2016), for earlier intervals there is a paucity of hominin-lacustrine related sites outside the East African Rift and southern Africa, other than those associated with Megalake Chad at ~ 7.3 Ma (Late Miocene) and ~ 3.6 Ma (Late Pliocene) representing the

* Corresponding author at: Lancaster Environment Centre, Lancaster University, Lancaster LA1 4YW, UK.

E-mail addresses: m.hounslow@lancaster.ac.uk (M.W. Hounslow), h.white.4@warwick.ac.uk (H.E. White), nick.drake@kcl.ac.uk (N. Drake), sjm11@leicester.ac.uk (S.J. McLaren), ahmed.elhawat@uob.edu.ly (A.S. El-Hawat).

westernmost presence of Pliocene hominins (Lebatard et al., 2008; Su, 2024). Fundamental conditions for hominin dispersal from the East African Rift, and particularly across a green Sahara, are likely to have been the availability of freshwater, which was strongly dependent on central Saharan lake systems (Mirazon Lahr, 2010), the Nile River or the Eosahabi River system sourced from Megalake Chad (Muftah et al., 2013). Neogene trans-Saharan lacustrine conditions likely also needed north to south climate synchronicity as desert conditions grew and diminished, stimulated by palaeoclimatic change.

In the Libyan Fezzan widespread post-Paleogene interbedded limestone and terrestrial siliciclastics were mapped by the Industrial Research Centre (e.g. Koráb, 1984; Parizek et al., 1984; Seidl and Röhlich, 1984; Fig. 1), and have been associated with Lake Megafezzan, which had a maximum size of $\sim 135,000 \text{ km}^2$ (Drake et al., 2008) with these sediments distributed over a large area of the Fezzan. We investigated many of these during fieldwork between 2005 and 2011 and recognised numerous extensive sedimentary sequences associated with evidence of humid intervals. These units are found on the fringes of the Awbari and Murzuq sand seas, occupying areas west and south of the flat lying to gently tilted Paleogene sediments forming the edges of the Sirte and Ghadames basins (Fig. 1). Hounslow et al. (2017) sub-divided these post Paleogene units in the Fezzan into the Shabirinah, Brak, Zarzur and Shati formations (Fig. 2) of the Al Mahrurah Group, in part following Thiedig et al. (2000). The Al Mahrurah Group occupied two large interconnected endoreic basins principally focussed on the Awbari and Murzuq sand sea regions, which had formed via deflation by the end of the Paleogene (Desio, 1971). The Shabirinah, Brak and Zarzur formations rest on various Paleozoic and Mesozoic basement rocks, generally lack suitable fossils for precise dating and have not been significantly affected by tectonism since deposition. Deposits of the youngest Shati Formation (Fm) are associated with Late Pleistocene age stone tools at lake marginal situations having been more precisely dated (Mattingley et al., 2003; Armitage et al., 2007; Mirazon Lahr, 2010; Drake et al., 2018).

Several dating methods have been used to understand the chronology of the Al Mahrurah Group, including ^{14}C , luminescence techniques, U/Th disequilibria dating, and magnetostratigraphy (Gaven et al., 1981; Geyh and Thiedig, 2008; Hounslow et al., 2017; Drake et al., 2018). The

former methods provided robust chronology for the late Pleistocene Shati Fm (Fig. 2), which represents the deposits of several smaller lake systems (Drake et al., 2018). The Shati Fm, and its locally developed lower part, the Aqar Member (Mb) formed largely during marine isotope stage (MIS) 5 (Causse and Hillaire-Marcel, 1988; Drake et al., 2018). The distinctive Aqar Mb comprises *Cerastoderma glaucum* dominated coquinas formed as shoreline deposits in Palaeolake Shati during MIS 5 (Petit-Maire et al., 1980; Petit-Maire, 1994; Gaven et al., 1981; Rosso and Gaillard, 1982; Drake et al., 2018). The shoreline deposits of Palaeolake Shati are associated with middle stone age (Aterian) tools although earlier tools are also widespread in Wadi ash Shati and wider in the Fezzan (Petit-Maire, 1982; Mattingley et al., 2003; Foley et al., 2013; Cancellieri, 2021). In contrast the magnetostratigraphy of Hounslow et al. (2017) provides a chronology for the Early and Middle Miocene Shabirinah and Brak formations (Fig. 2). These represent the deposits of once-extensive carbonate lakes, fluvial and dryer terrestrial environments, with likely riverine outflow eastwards into the southern part of the Sirte Basin (Fig. 1).

The focus of study here is the Zarzur Fm, which is sandstone dominated, but contains carbonates especially in the Bir az Zallaf Mb (Fig. 2), which together expand the sedimentary record of lake deposits in the Fezzan into the Upper Miocene and Pliocene in the formation type-area in Wadi ash Shati (Figs. 1, 3). The aims here are to: 1) build a chronology for the Zarzur Fm using magnetic polarity stratigraphy; 2) evaluate the depositional conditions represented by the Zarzar Fm, at both section-scale and over the Wadi ash Shati region; 3) discuss likely hydrological conditions that sustained lacustrine units in Wadi ash Shati, based partly on carbon and oxygen stable isotope data and 4) assess the implications of these lacustrine deposits for the green Sahara hypothesis, and possible equitable early hominin habitats.

2. Methods

2.1. Fieldwork and sampling

We logged and sampled six sections over two field seasons (2007, 2011; Table 1). These results were integrated with two additional sections west of our study sites as studied by Abdullah (2010).

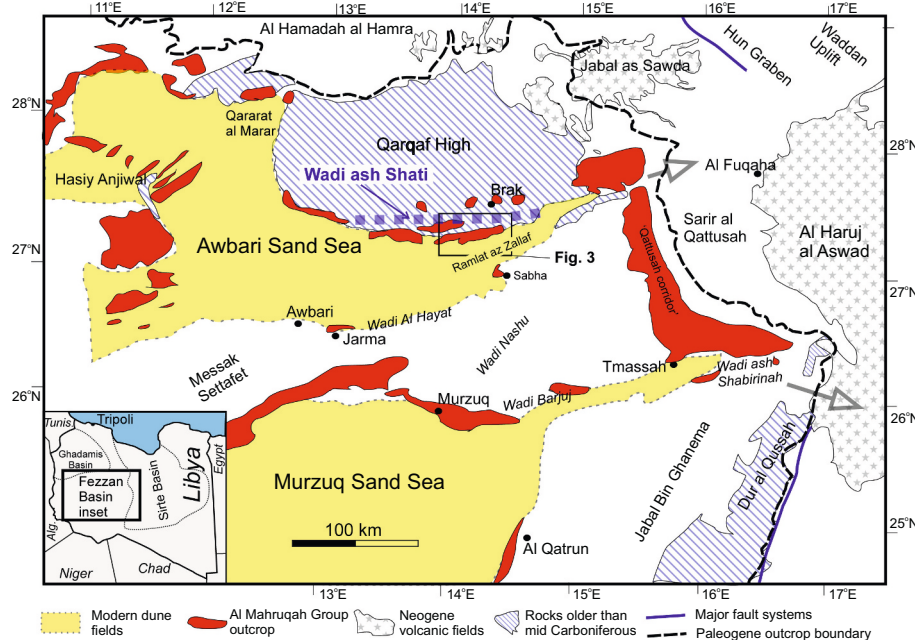


Fig. 1. Outline geology of the Fezzan with study area location labelled as Fig. 3. The position of Wadi ash Shati is indicated by a blue dashed line. Large grey arrows are hypothesised drainage exits from the Fezzan Basin referred to as the northerly Wadi Nashu, and easterly Wadi Barjij exit (Drake et al., 2008, 2011). Map simplified from IRC (1985). (For interpretation of the references to colour in this figure legend, the reader is referred to the web version of this article.)

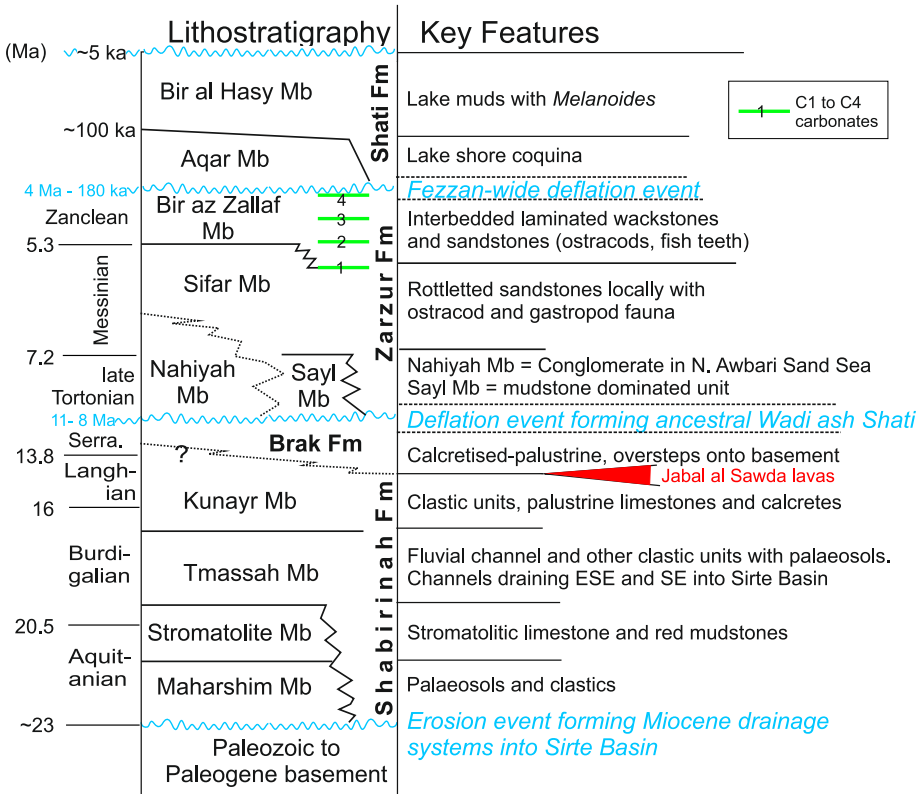


Fig. 2. Lithostratigraphy of the Al Mahrurah Group in the Fezzan, with major events and features indicated (adapted from Hounslow et al., 2017). Major erosion/deflation events indicated (in blue) sub-divide the formations. Zarzur Formation ages are based on this work; other formation ages from Hounslow et al. (2017) and Drake et al. (2018). Estimated durations of hiatuses are in blue. (For interpretation of the references to colour in this figure legend, the reader is referred to the web version of this article.)

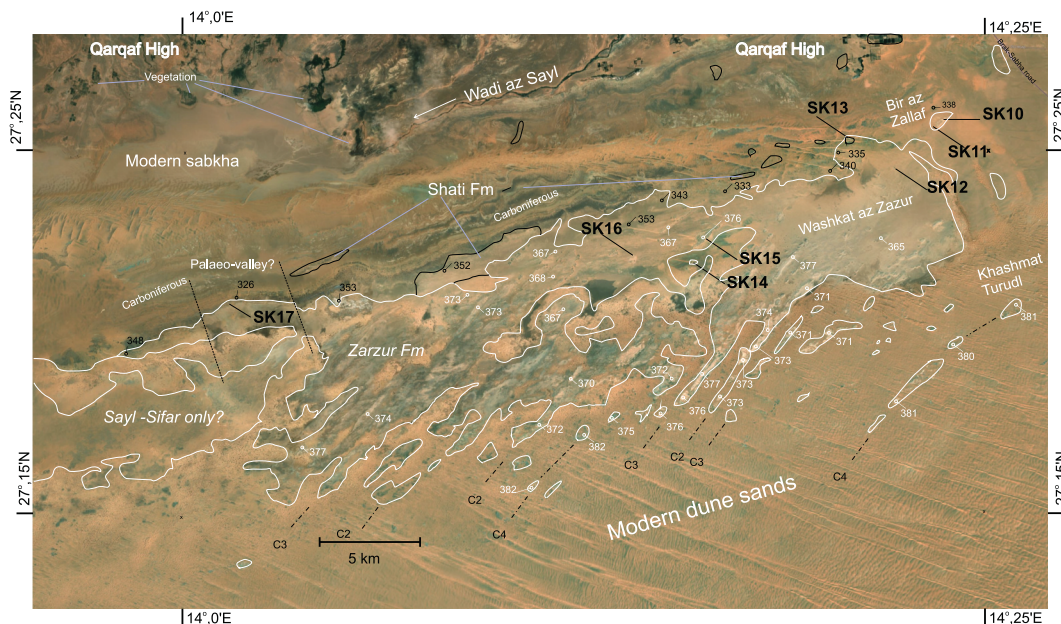


Fig. 3. Satellite image of southern Wadi ash Shati (from bing.co.uk) overlaid with Zarzur Formation (white outline) and Shati Formation outcrops (in black lines) (from Seidl and Röhlich, 1984). Site name codes used here (SK10-SK17) are as in Hounslow et al. (2017). The northern part comprises Early Carboniferous basement (partially covered by sand and modern Sabkhas), and the southern parts are covered by modern dunes. Selected spot heights of plateau tops (in white) corresponding to the C2 to C4 carbonates in the Bir az Zallaf Member (C4 inferred). Black spots heights are on basement outcrops close to the base of the Sayl Member, which generally become lower to the SW of the outcrop area at around SK17. A NE to SW plateau ridge alignment is apparent in the eastern outcrop marked by dot-dash lines.

Table 1

Studied sections in Wadi ash Shati. GE = Google Earth. The locations of sections SK16, SK17 have been moved to the likely Google Earth location, based on photographs and approximate locations of [Abdullah \(2010\)](#) and Google Earth imagery.

Site name	GE location (latitude: longitude)	Members	Reference
SK10	N27°,25',57.9": E14°,33',27.3"	Sayl, Sifar, Bir az Zallaf	This study
SK11	N27°,25',48.4": E14°,23',13.1"	Sayl, Sifar, Bir az Zallaf	This study
SK12	N27°,24',38.2": E14°,21',58.1"	Sifar	This study
SK13	N27°,25',29.4": E14°,20',36.1"	Base of Sayl	This study
SK14	N27°,22',04.0": E14°,15',48.9"	Sifar, Bir az Zallaf	This study
SK15	N27°,22',43.6": E14°,16',12.1"	Sifar, Bir az Zallaf	This study
SK16	N27°,22',16.0": E14°,13',53.0"	Sifar, Bir az Zallaf	Abdullah (2010)
SK17	N27°,20',56.0": E14°,01',37.0"	Sifar, Bir az Zallaf	Abdullah (2010)

Samples were principally collected from the measured sections for magnetostratigraphic dating. Hand-samples were exclusively used because lithologies (except carbonates) were friable and prone to disintegration. In the field, samples were prepared into $\sim 15 \times 15 \times 15$ cm monoliths, using hammers, chisels and knives (Hounslow et al., 2022). Soft and friable lithologies were impregnated with waterglass (sodium silicate solution; Kostadinova et al., 2004) *in situ* in the field and left to dry overnight. Each sample was prepared with a suitable flat surface on which the footprint of a specially designed orientation staff was marked, and oriented using a magnetic compass (Hounslow et al., 2022). In the laboratory, many samples were re-treated several times with water glass to consolidate them sufficiently for specimen cutting (Kostadinova et al., 2004). After sufficient drying (at room temperature) the treated blocks were re-oriented in dental plaster, and a diamond saw was used to cut 2.2 cm cubic palaeomagnetic specimens. Most specimens were cut dry, with additional intermediate stages of waterglass application to further consolidate sample slices and cubes. Bedding was horizontal, although some locally undulating bedding attitudes were measured in the Bir az Zallaf Mb carbonates. Three samples fragmented in transit and failed to yield specimens. Palynological analysis was attempted on additional samples, but none yielded pollen.

2.2. Magnetic measurements and data analysis

In total 76 samples (labelled in Fig. 4), were collected from four sections yielding 159 measured specimens. The specimens were predominantly demagnetised using only thermal demagnetisation (using a Magnetic Measurements Ltd. thermal demagnetiser, with field cancellation to <5 nT). However, an initial set (21 % of all specimens) used a combined scheme with initial thermal demagnetisation to 230–410°C followed by reversing, tumbling alternating field (AF) demagnetisation to around 80 mT in 5–10 mT steps (using a Molspin AF demagnetiser). This combined AF demagnetisation proved effective at demagnetising the natural remanent magnetisation (NRM) intensity, but initial assessment suggested poor separation of magnetisation components, and hence thermal magnetisation alone was used for later specimens. The NRM of each specimen was measured using a CCL GM400 3-axis cryogenic magnetometer (practical measurement noise limit ~ 4 $\mu\text{A}/\text{m}$; Supplementary Information (SI) Fig. S7a) using 3 specimen positions, with automatic holder magnetisation removal. The magnetisation measurement precision was determined using the γ_{95} of Briden and Arthur (1981) from 12 measurements of each XYZ direction (γ_{95} is comparable to the more familiar Fisher distribution α_{95}). From each sample 2 or 3 specimens were measured (SI Fig. S7c). Median specimen

NRM intensity and magnetic susceptibility are 0.78 mA/m and 2.7×10^{-5} SI, respectively. In general, thermal demagnetisation was conducted in 100°C increments from room temperature to 300–400°C and then in 30–50°C increments to 580 to 630°C or until the specimen γ_{95} approached the effective noise level ($\sim 40^\circ$; SI Figs. S7a, S8). Magnetic susceptibility (κ) was measured after each heating stage to monitor for mineralogical changes (measured using a Bartington Instruments MS2 susceptibility meter). Specimens were kept in mu-metal boxes (residual magnetic field <20 nT) between demagnetisation and measurement steps.

A two-category classification is used to express; 1) the often complex demagnetisation behaviour and 2) quality of the inferred polarity. The merits of such qualitative classifications are discussed by Hounslow et al. (2022). Based on stereographic projections and Zijderveld plots (Zijderveld, 1967) demagnetisation behavioural categories were assigned to specimen data, with specimens qualitatively classified into either S or T-class (a classification like Montgomery et al. (1998) and Hounslow et al. (2004)), based on effective isolation of the characteristic remanent magnetisation (ChRM). S-class specimens had suitable linear trajectory ChRM line fits and were subdivided into three classes (S1, S2, S3, with S1 being best quality) based on the length and qualitative isolation of the ChRM. For these classes a breakdown of α_{95} for the line fits are given in SI Fig. S13e. T-class behaviour have great-circle type trends indicating incomplete separation of the ChRM, with three qualitative sub-divisions (T1, T2, T3) based on the scatter, demagnetisation path length and approach to expected ChRM. The T1 class approaches the expected ChRM (α_{95} for plane fits in SI Fig. S13f). Many example demagnetisation diagrams are given in SI Fig. S11. A final class (X) is assigned to specimens that contain no evident ChRM, either due to excessive directional scatter or dominating overprints. Specimen magnetisation directions were quantitatively evaluated using LINEFIND (Kent et al., 1983, DOSBox version; Hounslow, 2023a), a more sophisticated version of the standard principal component analysis. This utilises the measurement variance and/or a smoothed model of that variance, with an excess standard deviation fitting parameter (ρ), selected by inspection and guided by the Akaike information criterion. The advantages of using the LINEFIND approach are outlined in Hounslow et al. (2021).

Polarity quality classification is assigned based on demagnetisation plots and ChRM behaviour with the following sub-categories of descending quality of normal (N) and reverse (R) polarity: N, N?, N??, R, R?, R?? A final category of "U" indicates that no ChRM polarity could be reliably inferred. Based on the number of specimens, demagnetisation behaviour and polarity quality, magnetozone widths of $1/3$ to full width represent a qualitative confidence indicator. Directional means, reversal tests and specimen relative virtual geomagnetic pole latitude (VGP_R; Hounslow et al., 2022) determinations were made using the PalaeomagTools software (Hounslow, 2023b).

2.3. Statistics of polarity correlations

Magnetostratigraphic dating relies on a correlation to the geomagnetic polarity timescale (GPTS). Possible polarity correlation options were quantified using statistical similarity indices of: a) the similarity of matrices index, b) Procrustes similarity index and c) the distance correlation statistic (Székely and Rizzo, 2017; Indahl et al., 2018). These multivariate statistics used five variables to characterise each magnetozone and GPTS chron: t_0 (thickness, or duration), $\log_e(t_{+1}/t_0)$, $\log_e(t_{-1}/t_0)$, polarity bias, and Shermans ω_2 statistic. The latter four variables use t_{+1} , t_{-1} , the corresponding values for the overlying and underlying magnetozones/chrons and t_0 . The \log_e ratio values have less dependency on sedimentation rate changes (Man, 2008, 2011), and as such the statistical comparison does not assume conformity of sedimentation rates as in 'classical' simpler methods (see discussions in Man, 2011; Lallier et al., 2013). Polarity bias and ω_2 are indicative of more local polarity structure than t_0 or \log_e indices individually (Olson et al.,

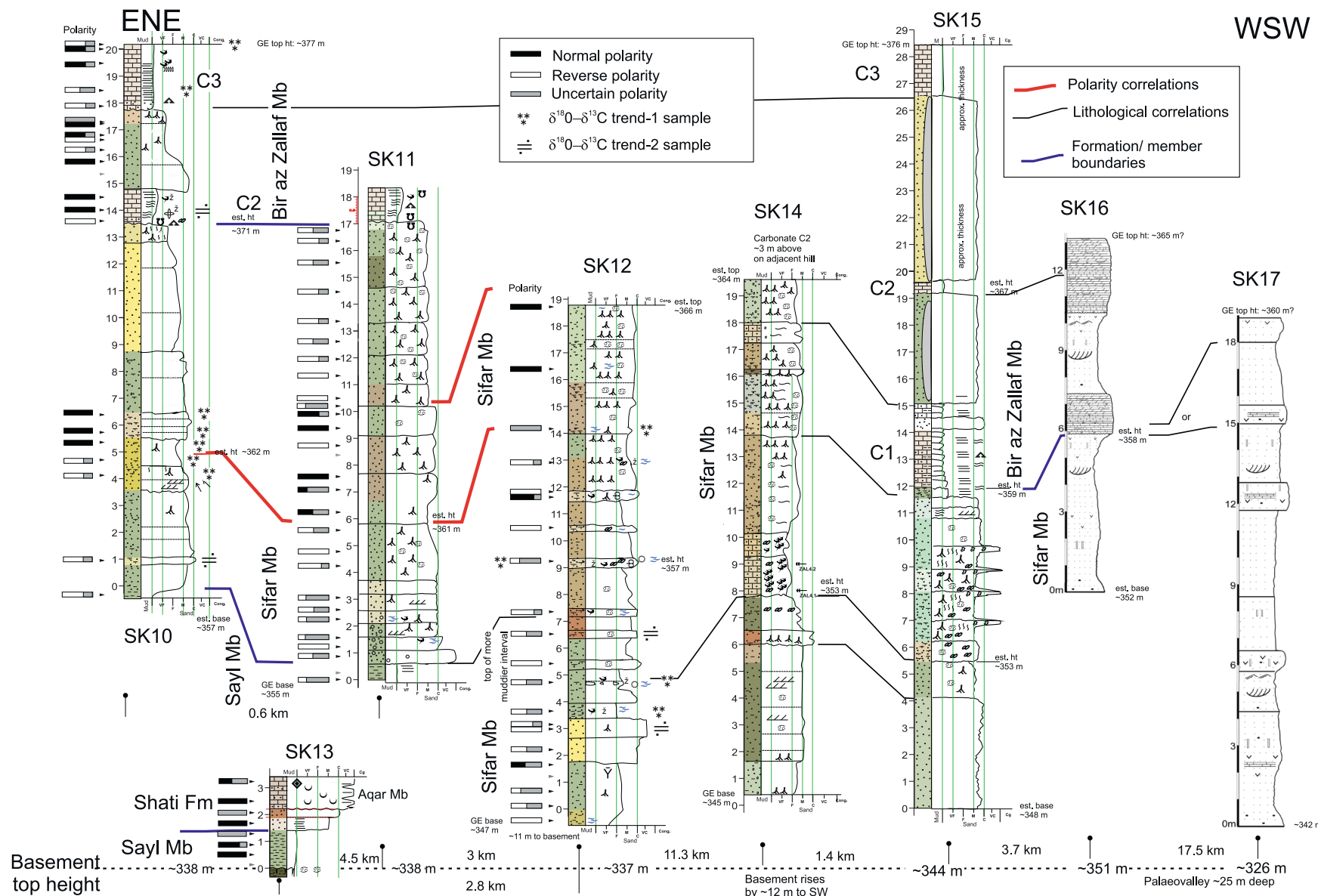


Fig. 4. Regional correlation of our logged sections and two sections (SK16, SK17) from Abdullah (2010). Section logs and summary magnetic polarity data for the sections (key to logs in SI Fig. S6). The width of the bar in the polarity boxes indicates the confidence in the horizon polarity obtained from the two to three specimens from each sample level. Kilometre distances at the bottom are distances between outcrops. GE = Google Earth elevations. ‘est. ht’ = estimated elevations.

2014) and have been used in quantitative multivariate polarity correlation assessments (Hounslow et al., 2022). The probability of association of corresponding polarity patterns uses the RV-based statistic P_{RV} , and permutation test for distance correlation giving P_{dCor} (Székely and Rizzo, 2017; Josse and Holmes, 2016). These statistics were determined using R (R Core Team, 2022).

2.4. Petrography and stable isotope methods

Thin sections were prepared from the palaeomagnetic water glass impregnated samples. Initially slices were cut, cleaned and dried. Araldite DBF resin (and XD716 hardener) and Araldite DW blue colouring were used to highlight pore spaces. Glue was poured over the samples, placed in a vacuum for about 15 min, and left to set. To overcome a waterglass efflorescence forming during glueing of the slice to glass slides, the Araldite impregnated slices were soaked in water for about 10 min, then dried. This extracted much of the waterglass from the slices. The 30 µm thick, thin-sections were made with a Logitech LP50 Precision Lapping & Polishing System. A few were made by Petrolab Ltd. and Wagner Petrographic, USA. Observations were made using a Nikon Eclipse LV100ND microscope fitted with a Nikon Digital Sight DS-Fi2 camera.

Selected sub-samples containing little or no waterglass were assessed for carbonate $\delta^{18}\text{O}$ and $\delta^{13}\text{C}$. A sub-sample was powdered using a pestle and mortar and a fraction was wet-sieved with deionised water through a 75 µm sieve (Gasse et al., 1987; Anderson and Leng, 2004). The <75 µm fraction contained most of the carbonate and wet sieving additionally removed the waterglass into solution. This fraction was filtered and oven dried for 4 h at 65°C and then placed in a Mini Lyotrap freeze drier for >24 h to assure complete moisture loss. The dried sample was powdered in a ball mill. CO₂ from acidified samples was produced in a Gilson autosampler system. A ~2 mg sub-sample was used in the analyses, although those with a low CO₂ content were re-run with a greater amount. Labco Ltd. Exetainer® glass vials containing the sample were flushed with He to remove air and then acidified with ~0.2 ml of 100 % phosphoric acid (prepared following McCrea, 1950) and left at 50°C for three hours to equilibrate before measurement. Seventeen samples were analysed using a SERCON Hydra 20–20 continuous flow isotope ratio mass spectrometer. Calibration used the IAEA calcite standard CO8, and values are based on means from triplicate sub-samples. The precision was 0.08‰ for $\delta^{18}\text{O}$ and 0.04‰ for $\delta^{13}\text{C}$ (per mil, ‰, VPDB).

3. Sedimentology of the Zarzur Formation

Observations from our fieldwork in Wadi ash Shati showed that the Zarzur Fm consists of the Sayl, Sifar and Bir az Zallaf members (Fig. 2). Outcrops occur on the flanks and tops of often linear plateaus, which have a NE-SW orientation (Fig. 3). Topographic lows between plateaus are generally covered by aeolian sand, weathered regolith and/or small playas covered in halite and gypsum crusts. The Zarzur Fm in Wadi ash Shati is un-tilted since deposition. Evidence for this is based on three carbonates (C2 to C4) of the Bir az Zallaf Mb visible on remotely sensed images, and a lower fourth one only seen in sections (carbonate C1). These carbonate units, which typically cap plateau tops in the SE of the outcrop area, have a consistent height based on elevations derived from Google Earth (Fig. 3).

The studied sections consist of limestones, sandstones and sandy mudstones. However, there is a high degree of lateral variability of siliciclastic lithologies which makes it difficult for precise lithological correlation between sections, even those less than 1 km apart. The most robust lithological markers are the Bir az Zallaf Mb carbonate units. Other less reliable markers are the sandstones lower in the Zarzur Fm that tend to be slightly siltier, with the youngest sandy mudstones marking the top of the Sayl Mb. Gastropod- and ostracod-rich sandy levels are also potentially useful for correlation, occurring in some sections of the Sifar Mb (i.e. SK12, SK14, SK16; Fig. 4). Robust inter-section

correlations were achieved in the Sifar Mb using lithological changes, assisted by the sample magnetic polarity (Fig. 4). In the east of the outcrop area shown in Fig. 3 (not investigated by us), the lack of substantive carbonate units evident in Google Earth imagery suggests that the Bir az Zallaf Mb is absent, either due to its erosion, or because carbonates within it are absent in that area. Section SK17 (in the Sifar Mb; Fig. 4) has thinner, barely laminated sandy dolomitic beds, with underlying teepee-like deformation, like the lower contacts of the C2 and C3 carbonates (Fig. 4; Abdullah, 2010). Section SK13 has a sandy mudstone at the base of the Sayl Mb, sitting on a fissured and calcrete-bearing muddy unit of the underlying Carboniferous (Figs. 4, 5C). These calcrites indicate a weakly developed palaeosol at the unconformity. At the same stratigraphic position elsewhere in Wadi ash Shati, Cole and Riser (1982) describe a 0.5–1 m thick, carbonate-cemented (pink coloured) sandy conglomerate/breccia comprising well-rounded limestone and Paleozoic clasts. This is likely a coeval calcretised gravel at the boundary. Around 11 m of the poorly exposed Sifar and Sayl members lie between section SK13, and the overlying and nearby SK12 section (Figs. 3, 4). Depositional processes of the younger Shati Fm have cut-into and eroded much of the lower part of the Zarzur Fm in this area of Wadi ash Shati, which has obscured outcrop at this level (Figs. 3, 4, 5C).

3.1. Lithofacies

The characteristics of the sections examined in the field and interpretation of thin-section data reveal eight lithofacies in the Zarzur Fm (Table 2). These are named according to the lithofacies codes from Farrell et al. (2012), with addition of S og (ostracod and/or gastropod rich sandstone), and peloidal carbonate (C p), as outlined below.

Lithofacies gS: Pebby and granule-bearing coarse and medium-grained sandstone occurring near the base of the Sifar Mb at section SK11 (SI Fig. S1a), between 6.5 and 8.5 m in SK10, and at 3.5–4 m in SK12 (Fig. 4).

Lithofacies S x: Cross-bedded, often friable, medium to coarse sandstone, best developed at ~4 m in section SK10, and at 3–5 m in section SK14 (Fig. 4). The cross-bedding, lack of fines and largely uncemented nature are characteristic of this facies (SI Fig. S2d).

Lithofacies S m: This is the most common facies of the Zarzur Fm (Fig. 5F; SI Figs. S3c, e). It consists of fine to coarse sandstones, often lacking structures, but frequently containing small amounts of incipient mm-cm sized calcrete micronodules and lenses. Framework grains are generally bimodal in size with well-rounded coarser grains dispersed within more angular medium and fine sand (Fig. 5D, SI Fig. S2b). Grains are predominantly quartz, with lesser amounts of microcline, with minor chert and quartzite lithoclasts (SI Fig. S2a). Widely spaced mud-cracks occur in section SK12 at 1.5 m (SI Fig. S3e). Occasional argillaceous aggregates occur as sand-sized clastic particles, as observed in other desert settings, which result from fragmentation and remobilisation of surficial soils as mud aggregates on floodplains (Rust and Nanson, 1989; Magee et al., 1995; Muller et al., 2004).

Facies mS m: Very fine to medium-grained muddy sandstones lacking sedimentary structures but in places containing shell fragments and rare ooids or rhizoliths. The former suggest proximity to aquatic habitats.

Facies S rt: Calcareous sandstone of medium to coarse-grained texture with extensive bioturbation and rhizolith development. Associated microfossils include occasional foraminifera and ostracods (Fig. 5D). Foraminifera are widely described from modern and Holocene lake successions in the Sahara, transported to lakes by migratory birds (Gaven et al., 1981; Petit-Maire, 1989; Abu-Zied et al., 2011). Sandstones are patchily cemented by intergranular pore-filling microspar and meniscus calcitic cements (Fig. 5D, SI Fig. S2b). Localised micritic cements express the frequent incipient calcrete micronodules and lenses in the sandstones. These are preferentially associated with rhizoliths (SI Fig. S4d) and occasional gypsum cements (SI Fig. S4e).

Facies S og: Medium to coarse sandstone with trace to large amounts

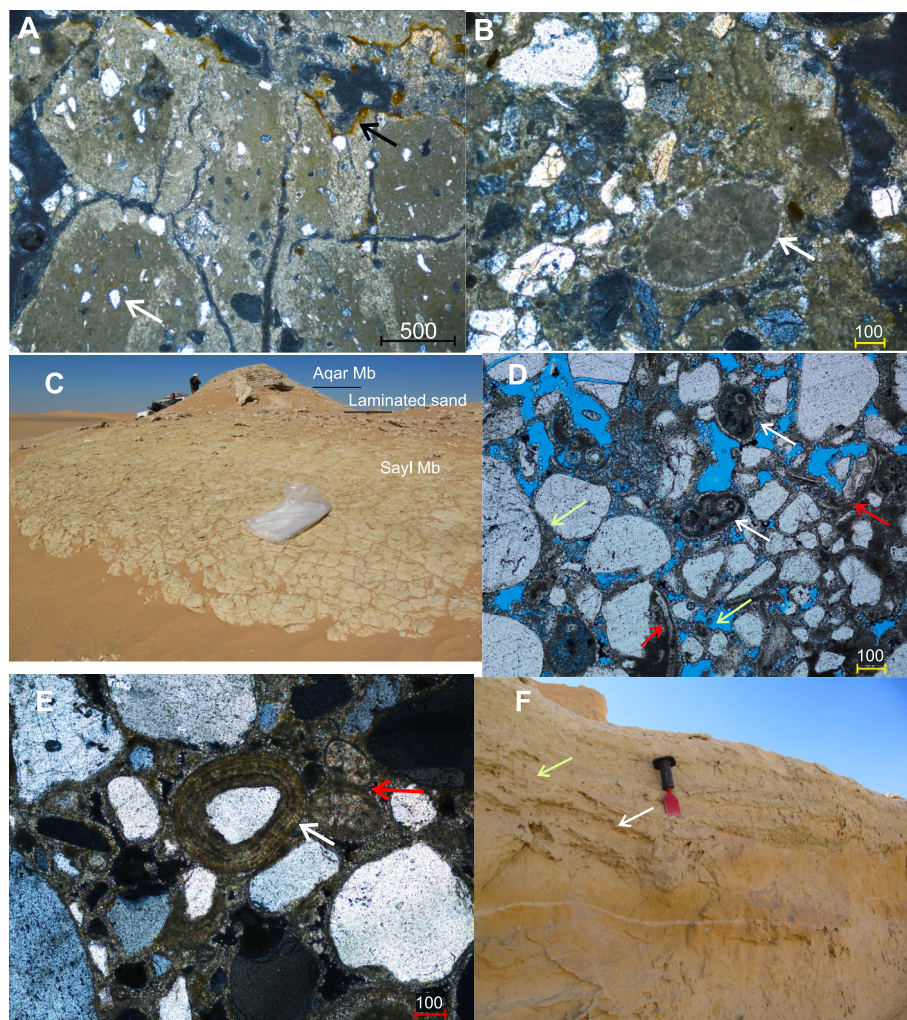


Fig. 5. Sedimentological and petrographic details of the Sayl and Sifar members. A, (AL12, SK10 section, facies sM). Sandy siliciclastic mudstone of the Sayl Member (sand grains indicated with white arrow). The cracks are largely from modern outcrop desiccation, but also from drying in the laboratory to stabilise samples for specimen preparation. Reddening along some cracks (black arrows) is probably a result of modern oxidation, since no primary reddening is apparent in the Zarzur Fm in Wadi ash Shati. B, (AL12, SK10 section, facies sM). Siliciclastic mud aggregate (arrowed) amongst quartz grains in a muddy matrix, with micritic rims, and probably disrupted aggregates immediately above the arrowed one. C, The SK13 section at the base of the Sayl Mb, with overlying laminated sand and *Cerastoderma glaucum* coquina (i.e. Aqar Mb) of the Shati Fm. The Carboniferous basement is hidden in the blown sand in bottom left. D, (BZ90, SK12 section, facies S rt). Foraminifera (white arrows), with fragmented ostracods (red arrows) in a bimodal grain sized sandstone, with meniscus and rim micritic cements on the clasts (green arrows). E, (ALA2, SK12 section, facies S og). Thick ooid cortex with a quartz particle core (white arrow). Two micritic peloid-like grains to the right (red arrows). F, (Section SK12). Lower part of a small cliff is a structureless sandstone (facies S m) overlain by a weakly cross-bedded sandstone (white arrow), which contains common rhizoliths (green arrow) that contain slightly more carbonate. Scale bars are in microns. (For interpretation of the references to colour in this figure legend, the reader is referred to the web version of this article.)

of ostracods and the gastropod *Melanoides tuberculata*. The sandstones are generally richer in pore-filling carbonate cements than other sandy facies (SI Fig. S3b), whilst some sandstones contain ooids, with quartz-clast cores that are particularly prevalent at 3.5 m, 4.8 m, 9.2 m and 13 m in SK12 (Fig. 4, Figs. 5E, 6A; SI Fig. S3a). Probable gyrogonites (calcified oogonia of charophytes) occur in section SK12 (SI Fig. S2c). Foraminifera also occur at two levels in SK11 (beds at 9.2 m and 11.6 m; Fig. 4). Section SK15 has a particularly abundant gastropod-bearing sandstone interval (composed of *Melanoides tuberculata*; SI Fig. S4a). Below the C1 carbonate bed in the SK15 section are sandstone beds alternating with *Melanoides*-rich intervals, which contain numerous likely reworked calcrete mini-nodules (SI Fig. S3d, S4a). In this facies ostracods are common and range in size from 300 µm to 1.1 mm (Fig. 6A). They typically have a thick micritic/microspar rim with the centre unfilled resulting in intraskeletal porosity. For much of the upper part of section SK12 microscopy reveals dispersed gastropod and ostracod fragments.

Facies sM: Green siliciclastic mudstones, with sand-sized quartz clasts dispersed within a largely homogeneous argillaceous matrix (Fig. 5A). Mudstones are typically fractured (Fig. 5C). In thin section occasional mud aggregates cemented by micrite rims occur (Fig. 5B). Some of the micrite may be filling micro-rootlet traces, which are not evident in hand specimens (SI Fig. S1b). The random mix of sand-sized and argillaceous material in this facies (Fig. 5A) is likely the result of original transport as a mixed quartz and mud pellet sand-grade sediment, in which original aggregates have been largely destroyed by burial, except for occasional examples of better preservation (Fig. 5B; SI Fig. S1b).

Facies Cp: This facies constitutes the C1 to C4 carbonate marker beds that punctuate the siliciclastic-dominated Bir az Zallaq Mb. These carbonates are well-bedded (Fig. 6B) and often well-laminated (Fig. 6F), with alternate carbonate-rich and fine-grained siliciclastic-rich layers (Fig. 6D; SI Fig. S5a). Biota range from charophyte aquatic plant remains and rhizoliths, lamellibranch shells, and fish bones (Seidl and Röhlich,

Table 2

Lithofacies and inferred depositional environments of the Zarzur Formation. Lithofacies codes are from Farrell et al. (2012), with addition of S og (ostracod and/or gastropod rich sandstone), and peloidal carbonate (C p).

Facies code	Description	Environmental interpretation
gS	Pebbly and granule-bearing coarse and medium-grained sandstones	Fluvial sand sheet
S x	Cross-bedded medium to coarse sandstone	Aeolian dunes
S m	Fine to coarse sandstones, often lacking structures, but containing zero to small amounts of incipient calcrite micronodules and lenses	Sandy playa and pedogenic-overprinted aeolian sandsheet
mS m	Very-fine to medium grained muddy-sandstones, lacking structures, but sometimes containing shell fragments and rare ooids or rhizoliths	Siliciclastic aquatic lake margin
S rt	Strongly rhizolith-bearing medium to coarse sandstones, with zero to small amounts of incipient calcrite micronodules and lenses	Vegetated dune flanks to subaerial margins of lake, with variable water table height
S og	Medium—coarse sandstone containing trace to large amounts of ostracods and (<i>Melanoides tuberculata</i>) gastropods	Siliciclastic lake
sM	Siliciclastic mudstones: green fractured siliciclastic mudstones with gypsum in which sand-sized clasts are dispersed within a largely homogeneous argillaceous matrix	Fluvially transported sand-sized mud aggregate
C p	Laminated and thin-bedded dolowackstones and dolo-mudstones	Carbonate lakes formed under variable salinity

1984; Geyh and Thiedig, 2008). Other features are wavy or contorted bedding, gypsum beds, fenestral texture, development of tepee structures and *in situ* brecciation (Fig. 6E, SI Fig. S5B). These features are consistent with lacustrine deposition under a wide range of salinities with intermittent periods of desiccation.

The thinly bedded carbonate layers have characteristic small-scale graded bedding motifs consisting of micritic peloids (Fig. 6C, D) passing into wackestone and dolomitic mudstone, with thin cavernous layers on top, indicating evaporite precipitation and dissolution. These mini cycles suggest deposition by waning flow, possibly induced by waves in a shallow lacustrine evaporitic setting. In places, peloids may coalesce to form aggregates joined by thin meniscus cement (SI Fig. S4c). These peloids lack internal structure and attain a clotted texture (Fig. 6C), which may suggest organic matter reworking in the mini cycle. Our sample staining with Alizarin Red S, and X-ray diffraction data (Abdullah, 2010) indicate that the carbonates consist of 80 to 90 % dolomite. Petrographic textural analysis of the carbonates indicates that dolomite is primary rather than from secondary replacement of a calcium carbonate precursor. Furthermore, the organic matter is likely an extracellular polymeric substance commonly formed in recent sabkhas, and evaporation ponds associated with sediments and microbial mats (Perri et al., 2018). These are pre-mineralisation materials that acted as a nucleation agent for mineral precipitation, such as silica and dolomite, as in modern hypersaline evaporitic conditions (Perri et al., 2018) but also recognised in ancient rocks (Perri and Tucker, 2007; El-Hawat et al., 2021).

4. Outcrop patterns of the Zarzur Formation

Many of the Zarzur Fm outcrops form elongated ridges oriented in a north-east to south-west direction and spaced at roughly equal intervals (Fig. 3). The spatial distribution of the outcrops was investigated using the Advanced Land Observing Satellite 30 m digital elevation model (DEM). In the DEM and Google Earth imagery the Zarzur Fm outcrops form flat-topped ridge features that emerge from under the modern

dunes and appear to reflect the original roughly parallel structure of inter-dune basin corridors (Fig. 7B). These are evident by the more resistant C2 to C4 carbonates that protect the ridges from modern wind erosion, often forming the plateau tops (Fig. 3).

An unlikely possibility is that the shape and spacing of Zarzur Fm outcrops reflect yardang development, with erosion following the average wind directions that Xia et al. (2024) demonstrated is near parallel to the Zarzur Fm ridges. However, if this were the case corridors between the Zarzur Fm ridges would cut into the underlying Carboniferous bedrock, for which there is no evidence. Instead, the local underlying Carboniferous tends to form small (a few metres wide) roughly equal-sized yardangs. The local Carboniferous bedding strike roughly parallels the base of the Zarzur Fm (Fig. 3). Furthermore, other formations of the Al Mahruqah Group nearby might be expected to have a similar ridge-like erosional pattern, yet they do not, as evidenced by the distribution of the Brak Fm on the northern margins of the Wadi ash Shati topographic basin, and the Shati Fm to the south (brown patches in upper Fig. 7A). In addition, at the fringe of the sand sea there is no evidence of emergence of a continuous carbonate sheet, which suggestss that these carbonate capped ridges reflect the internal structure of the Zarzur Fm, and not modern erosion (Fig. 3).

The orientation of modern large linear dunes and associated inter-dune corridors that dominate this part of the Awbari Sand Sea are NE to SW (Fig. 7A), the same direction as the Zarzur Fm outcrops, which suggests that they formed in a similar wind regime. However, the average modern interdune spacing is 2.91 km (standard deviation, SD = 0.37, number, n = 12), whereas the Zarzur Fm inter-ridge spacing averages 1.6 km (SD = 0.28, n = 7). Thus, ancient and modern inter-dune corridors appear to have differing widths, with the modern dunes being larger than those of the Zarzur Fm.

5. Magnetic polarity stratigraphy

Whilst there is lithological variety from mudstones to sandstones to dolostones, this variety does not strongly impact the quality of these rocks as palaeomagnetic field recorders, with similar behaviours throughout. This may reflect a general paucity of clay and siliciclastic silt fractions. However, carbonate-rich samples tend to have lower κ and NRM intensity, as evident in section SK10 (Fig. 8). The upper part of the Sifar Mb in section SK11 has notably lower κ and NRM intensity compared to section SK12 (Figs. 9, 10).

Directional behaviour of specimens from the four sections are also similar, so collective behaviour is described here. Three magnetisation components are evident, a low stability (LT) component (NRM to 100°C or sometimes 200°C; Fig. 11; SI Fig. S13a), an intermediate stability (MT) component and the ChRM (SI Fig. S13b). The ChRM component has a wide starting range, typically 200°C to 600°C, and an ending range often between 400°C and the origin of the Zijderveld plot (Figs. 11, SI S12b). LT and MT components are apparent as linear segments on Zijderveld plots, and occur in 85.5 % and 77.4 % of specimens, respectively, and tend to dominate the NRM (Fig. 11). The ChRM component is identified in 81.1 % of specimens, with 27.7 % S-class and 53.5 % T-class behaviour specimens (SI Fig. S13e,f). 18.9 % of specimens failed to yield reliable polarity information. In the final assessment, the combined demagnetisation scheme proved as effective as thermal demagnetisation alone, with 30 % and 70 % assigned to S-class and T-class data (Figs. 8c, 9c, 10c), compared to 27 % and 73 % when utilising thermal demagnetisation alone. The combined scheme typically produced starting ranges for the ChRM from 200 to 300°C and ending by 25–60 mT or more rarely the origin (SI Fig. S12b). The LT component is often a steep downward-directed component, which is more southerly displaced than the Brunhes age field for Wadi ash Shati (SI Fig. S13a, with mean PCA dispersion of $\alpha_{95} = 15^\circ$). The MT component, although strong in many specimens has no consistent direction, and is statistically random (SI Fig. 13b, with mean PCA dispersion of $\alpha_{95} = 13^\circ$). The LT and MT components are like those determined from the Miocene Shabirinah Fm

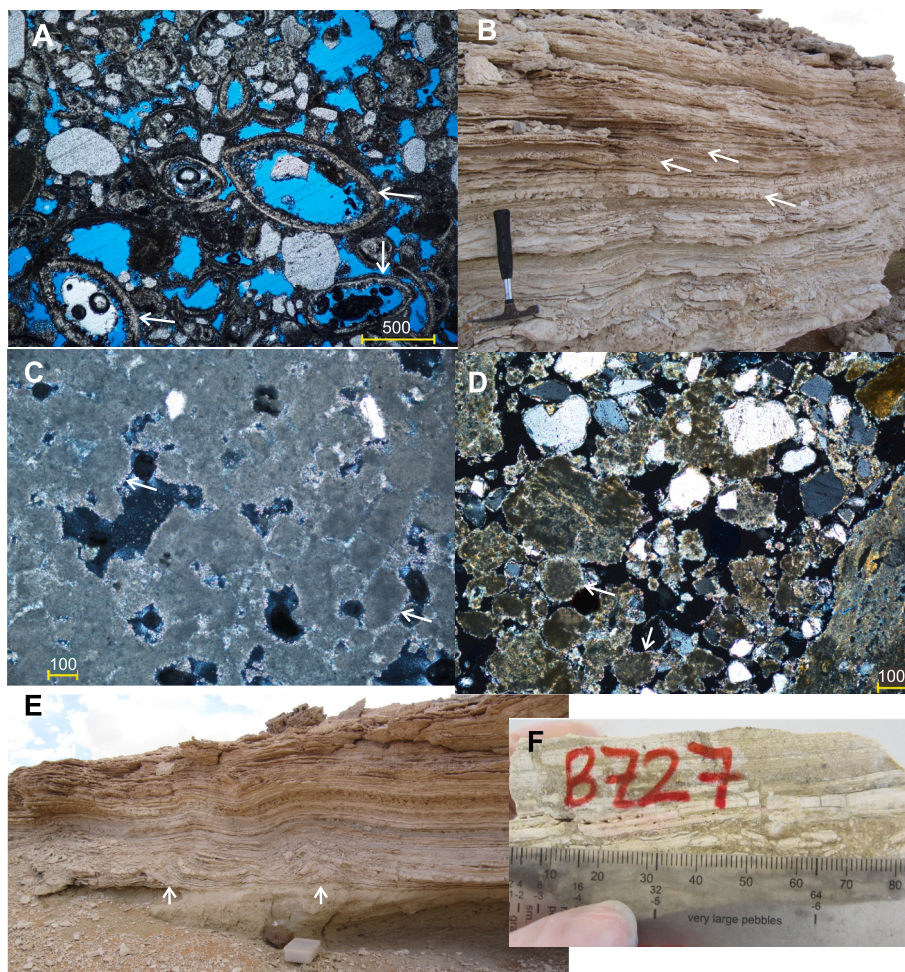


Fig. 6. Sedimentological and petrographic details of the Sifar and Bir az Zallaf members. A, (BZ91, section SK12, facies S og). Cluster of complete ostracod valves in a sandstone with open pore space. B, Bir az Zallaf carbonate C3 (section SK10), with thinly-bedded to laminated characteristics, and a generally upward decrease in siliciclastic content. The cm-thick beds alternate between continuous beds and vug-rich-beds (arrowed), which may have either contained former evaporites, or may contain dolomitised calcite. C, (BZ27, SK10, top of C2 carbonate, facies C p). Rounded peloids (arrows) joined by rim cements. Larger more irregular carbonate mud aggregates also present (crossed polars). D, (AL2, SK10 section, C3 carbonate, facies C p). Open-textured carbonate mud, with peloids (arrows) and sand-silt siliciclastics. Open pores are lined with micritic rim cements. These textures are representative of the more vug-rich beds as in B. E, (C3 carbonate, SK10 section). Two teepee structures (arrows) with a core of disrupted carbonate, which likely indicates evaporitic expansion. F, (BZ27, SK10 section, carbonate C2). Typical macroscopic lamination in carbonates, with alternation of purer and more argillaceous peloidal micrite, with disruption from desiccation or rootletting (vertical darker argillaceous veins).

in the Fezzan (Hounslow et al., 2017), and the LT component is likewise inferred to be largely a Brunhes age component, likely partially overlapping the ChRM. The origin of the random MT component is unclear.

From all specimens 26.4 % are inferred normal polarity and 54.7 % have reverse polarity (Figs. 8d, 9d, 10d). S-class directions when inverted to normal polarity yield a mean of $010.4^\circ/46.8^\circ$ and pass a reversal test with class Rc (Table 3; SI Fig. 13c). To determine a location-specific directional mean, the line and great circle fits were combined at the sample-level (method of McFadden and McElhinny, 1988) to determine sample means (Fig. 12), and a location sample mean, which has slightly steeper inclination at $006.2^\circ/50.8^\circ$ but likewise passes a reversal test with class Rc (Table 3). This was used to determine the VGP_R values shown in Figs. 8e, 9e, 10e. Using only the specimen great circle data produces a similar mean (SI Fig. 13d).

The basal Sayl Mb at section SK13 is of normal polarity (Fig. 4), whereas samples from the top of the member in sections SK10 and SK11 are dominantly reverse polarity (Fig. 4). The Sifar Mb is dominated by reverse polarity, except for normal polarity magnetozone ZA2n (Fig. 13A) in the mid part which is identified in all three sections (Figs. 8e, 9e, 10e, 13A). Two single sample normal polarity

magnetozones (ZA1r.1n and ZA1r.2n) occur in the lower part of the Sifar Mb, the lower of which is defined by two T-class specimens (Fig. 10c). ZA1r.1n is defined by two specimens from sample BZ84, the better quality one with polarity class N? (Fig. 10d). A single sample reverse submagnetozone occurs in ZA2n in section SK11 defined by two specimens (from sample BZ45), one with a confident 'R' class polarity (Fig. 9d). Accordingly, these single sample submagnetozones are assigned various widths corresponding to confidence of definition. The Bir az Zallaf Mb has a mix of normal and reverse polarity, which are reasonably well validated by the closer sample spacing in section SK10 (Fig. 8). A polarity composite is constructed by aligning the base of ZA2n in the three sections, although the boundary in section SK12 is ill-defined, with uncertain polarity sample BZ92 at the magnetozone boundary (Fig. 13A).

The Sayl Mb in sections SK10 and SK11 is clearly transitional into the base of the Sifar Mb as seen in section SK12 but magnetozone ZA1r.2n is not detected in SK11 (Fig. 13A), hence in the polarity composite this submagnetozone is reduced in relative thickness to match the closer sample spacing in section SK11 (Fig. 13A). In the polarity composite, the thickness of ZA2r is used from section SK11, because the upper

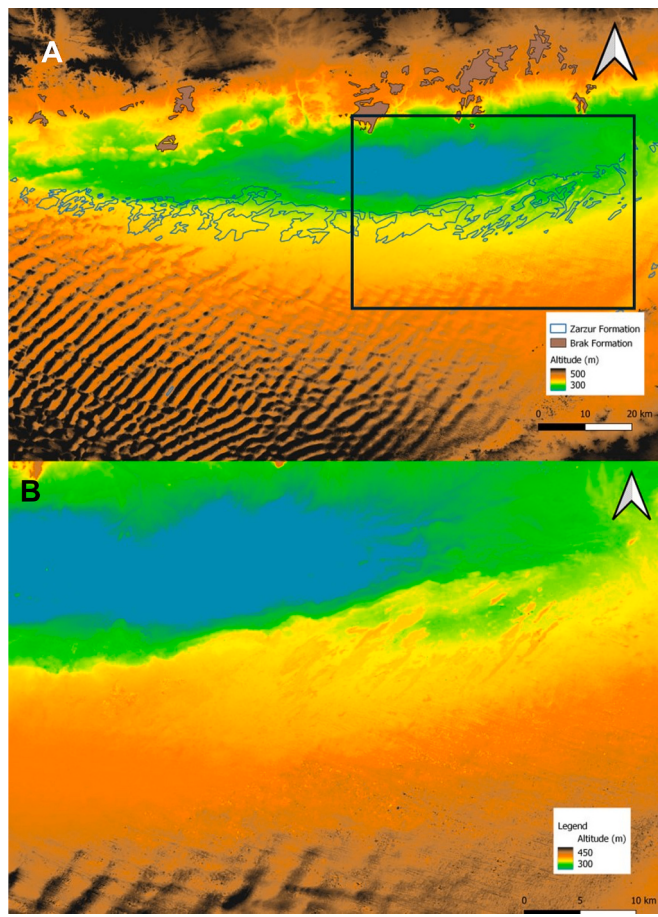


Fig. 7. A). Elevation structure in Wadi ash Shati, with generally NE-SW orientation of modern dunes in Ramlat az Zallaf, with outcrops of the Brak and Zarzur formations indicated. The Wadi ash Shati depression can clearly be seen sandwiched between the Qarqaf High and the outcrop belt of the Zarzur Fm. B). Close-up of the elevation (inset in A) in the Zarzur Fm with the NE-SW orientation of carbonate capped ridges of the Zarzur Fm outcrop. B covers the same area as Fig. 3.

boundary of magnetozone ZA2n is not defined in section SK10.

6. $\delta^{18}\text{O}$ and $\delta^{13}\text{C}$ of the carbonates and cements

Stable isotope data from the Zarzur Fm are limited, so additional data from the Aqar Mb of the Shati Fm in Wadi ash Shati are utilised from Gaven et al. (1981) and Geyh and Thiedig (2008) to better understand possible controls on lake hydrology and carbonate production (Fig. 14). Whilst younger than the Zarzur Fm, the similar palaeolatitude, and possibly similar water sources for both successions suggests that pooling the data may give a better understanding of $\delta^{18}\text{O}$ and $\delta^{13}\text{C}$ changes.

The Aqar Mb data from calcitic and aragonitic shells and calcitic cements (Gaven et al., 1981; Hillaire-Marcel, 1982) have essentially two primary carbonate groupings: ① $\delta^{18}\text{O}$, $\delta^{13}\text{C}_{\text{carb}}$ about 1‰ and 0.5‰, respectively and ② three samples about -5‰ and -4.5‰, respectively (Fig. 14). Grouping ② was shown by Gaven et al. (1981), Icole and Riser (1982) and Rosso and Gaillard (1982) to be the result of oligohaline water conditions recognised by an assemblage of *Corbicula africana*, *Coelatura lacoini*, *Bulinus truncatus* and *Lymnaea natalensis* from sections in eastern Palaeolake Shati (Petit-Maire, 1989). Their inference is supported by their sample locations within a delta and fluvial system on the eastern end of the lake depression (Icole and Riser, 1982; Drake et al., 2018), one of several riverine inputs suggested by Petit-Maire (1994). Similar faunal assemblages occur in the Bol region of modern Lake Chad

(Rosso and Gaillard, 1982).

Group ① samples (Fig. 14) are from the western part of Palaeolake Shati which Rosso and Gaillard (1982) and Petit-Maire (1989) showed are associated with euryhaline species (likely salinity range 3–30‰), but with ostracods indicating a more precise salinity range of 3–10‰ in well oxygenated waters (Petit-Maire, 1989). The western part was likely subject to more evaporation or longer residence times corresponding to larger $\delta^{18}\text{O}$ and $\delta^{13}\text{C}_{\text{carb}}$ (Horton et al., 2016). A third group (the recrystallised carbonate group; Fig. 14), comprising cements and shells was inferred by Gaven et al. (1981) to be a result of re-crystallisation of shell carbonate (giving lower Sr and higher Mg), but with similar $\delta^{13}\text{C}$ values to group ①, and lower $\delta^{18}\text{O}$ due to equilibration with pore waters during recrystallisation.

For the Zarzur Fm, many samples from sandstone cluster at around $\delta^{18}\text{O}$, $\delta^{13}\text{C}_{\text{carb}}$ of -8‰ and 2.5‰ and are associated with the meniscus cements connected to incipient calcrete nodules, indicating that the group probably reflects a groundwater source (groundwater cements cluster in Fig. 14). The $\delta^{18}\text{O}$ of these is around -8‰, comparable with a sub-cluster in the Aqar Mb recrystallised carbonate group, which may divisible into two sub-groups with $\delta^{18}\text{O}$ around -9‰ and -5‰. The later sub-group has similar $\delta^{18}\text{O}$ values to group ①. This suggest that some of the Zarzur Fm cements formed in similar lake-related groundwater $\delta^{18}\text{O}$ conditions as those from the Aqar Mb. This is borne out by the ostracod and gastropod bearing S og facies falling in this isotope cluster, and some from the mSm facies bearing ooids and shell fragments (facies codes on Fig. 14). However, a smaller group of three samples from the lower parts of the Zarzur Fm (from sandstones) have larger $\delta^{18}\text{O}$ between -1‰ to +0.5‰ (Fig. 14), but similar $\delta^{13}\text{C}_{\text{carb}}$ values to the groundwater cements group. This small cluster may relate to a fluvial related water source since evidence for fluvial input (facies gS with mud aggregates) is largely restricted to the Sayl Mb and lower parts of the Sifar Mb, the position of these samples (Fig. 4).

Samples from the Bir az Zallaf Mb carbonates (facies Cp) are widely spread throughout the $\delta^{18}\text{O}$ – $\delta^{13}\text{C}_{\text{carb}}$ range shown by the Aqar Mb and Zarzur Fm dataset, although these cluster at $\delta^{18}\text{O}$ values of around -5‰ and 2‰ (Fig. 14). These have $\delta^{13}\text{C}_{\text{carb}}$ largely greater than -1.5‰, except for one sample (Fig. 14). This wide variability in isotopic values for the Cp facies is not well-captured by the few spot samples and must be partially expressing a large $\delta^{18}\text{O}$ – $\delta^{13}\text{C}_{\text{carb}}$ variability within these carbonates. This is typical of modern north African Holocene lakes such as Lake Qarun (Egypt), where carbonate laminae have $\delta^{18}\text{O}$ variability of ~4‰ and ~3.5‰ in $\delta^{13}\text{C}_{\text{carb}}$ (Baioumy et al., 2011), but somewhat lower than observed in facies C p. Co-varying $\delta^{18}\text{O}$ – $\delta^{13}\text{C}_{\text{carb}}$ trends are typical of closed basins (Talbot, 1990; Li and Ku, 1997; Leng and Marshall, 2004; Horton et al., 2016), and accordingly there may be three possible trends in this combined dataset (Fig. 14), excluding the recrystallised carbonate group (Pearson correlation coefficient indicated).

Trend-1 (0.91): Mostly shown by $\delta^{18}\text{O}$ variation for the Aqar Mb samples, principally as *C. glaucum* shell material, but a few cement samples at lower $\delta^{18}\text{O}$. This trend extends into the groundwater cements cluster of the Zarzur Fm at low $\delta^{18}\text{O}$ and $\delta^{13}\text{C}_{\text{carb}}$. Two of the C p facies carbonate samples fall on this trend.

Trend-2 (0.86): Displayed particularly by the Cp facies and cement samples from low in the Zarzur Fm, a trend that extends into the (B) cluster of shell-data from the Aqar Mb. The three Zarzur Fm samples on this trend are from the lower parts of the Sifar Mb (Figs. 4, 14), where there are sedimentological indicators of fluvial sediment transfer such as pebbly sandstones and mud aggregates.

Trend-3 (0.81): Covariance between the (A) and (B) groups of the Aqar Mb, as expected if these groups represent geographically separated locations on the same lake system (or possibly different sub-basins), but with differing water inputs and salinity conditions.

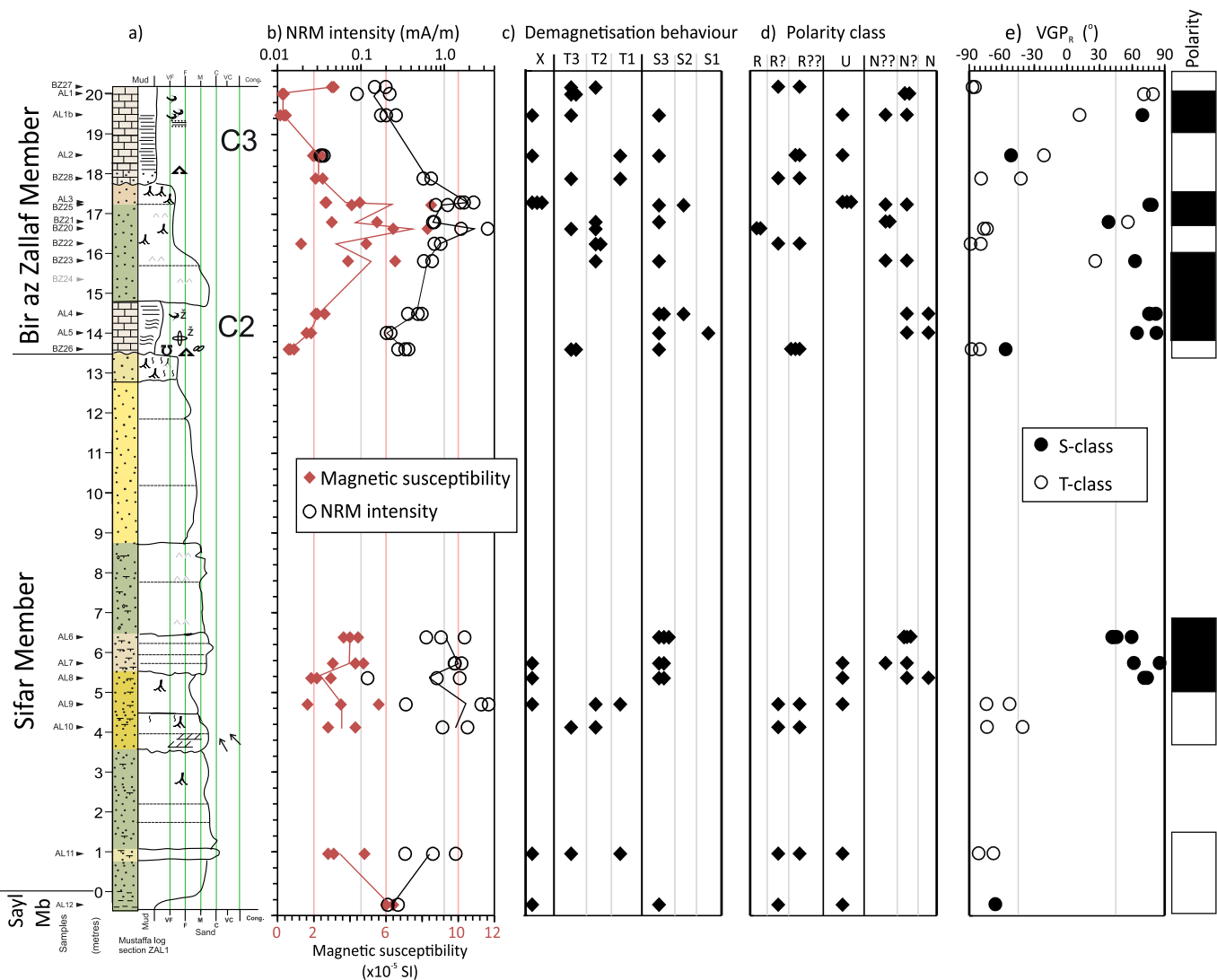


Fig. 8. Magnetostratigraphic data for section SK10. The columns are: a) lithostratigraphy, sedimentary log, sample positions and codes (those in grey yielded no specimens). b) Specimen natural remanent magnetisation (NRM) intensity and magnetic susceptibility (κ). c) Specimen demagnetisation behaviour with categorisation into good (S1) and poor (S3) ChRM line-fits; quality of great circle fit from good (T1) to poor (T3) (see text for details). d) Interpreted specimen polarity quality, with those in the U-column having unassigned polarity. e) Specimen VGP_R latitude, and section polarity. Polarity key as in Fig. 4.

7. Discussion and interpretation

7.1. Age of the Zarzur Formation

Saturated or near-saturated optically stimulated luminescence (OSL) dates from ~ 17.4 m (and from carbonate C3) in section SK10 suggest an age of ≥ 420 ka, which indicates that these successions are too old for OSL dating (Armitage et al., 2007). Extensive studies using $^{230}\text{Th}/\text{U}$ dating on carbonates (Thiedig et al., 2000; Geyh and Thiedig, 2008) yielded dates that are too young since the carbonates are unsuitable for U-Th or U-Pb chronology (Abdullah, 2010; Hounslow et al., 2017). The published biota from the Zarzur Fm are long ranging and do not provide a precise age for this unit, although a modern detailed study might provide better constraints. Hence, direct dating of the Zarzur Fm has been unsuccessful until now, and the magnetostratigraphic correlation to the GPTS is only constrained by older and younger limits from adjacent formations (Fig. 2).

An older constraint from the magnetostratigraphy of the underlying Brak Fm in Wadi ash Shati indicates that the Zarzur Fm is younger than Serravalian (Middle Miocene) in age, specifically chron C5An.1n at c. 12.2 Ma (Hounslow et al., 2017). However, the Brak Fm may extend to

younger than this, since the dating comes from a section in the lower to middle part of the Brak Fm, so possibly the uppermost parts may extend to 11–10 Ma. The termination of Brak Fm deposition must have been followed by a major time interval allowing some ~ 100 m of erosion to lower the floor of the ancestral Shati depression before deposition of the Zarzur Fm.

A younger age constraint is provided by the Shati Fm, with OSL dates from near the base in Wadi ash Shati of c. 130 ka (Drake et al., 2018). This is in accord with U/Th dates from the Aqar Mb which suggest a peak accumulation at 130 ka with some dates extending to 180 ka (Gaven et al., 1981). Therefore, the youngest reverse polarity sample in section SK10 places the section-top older than the base of the Brunhes normal polarity magnetochron (starting at 773 ka; Sugiyama et al., 2021). There was also a substantial time interval of erosion between the Shati and Zarzur formations, sufficient for creating a further ~ 50 m lowering of the Shati depression below the C4 carbonate of the Bir az Zallaq Mb.

With these constraints the pattern of dominantly reverse polarity in the Sifar Mb, and more closely spaced reversals in the Bir az Zallaq Mb, suggests three possible options for correlation to the GPTS, options A, B and C in Fig. 13B. These options differ in the detection of known magnetostrata, or the presence of possible spurious magnetozones (right-

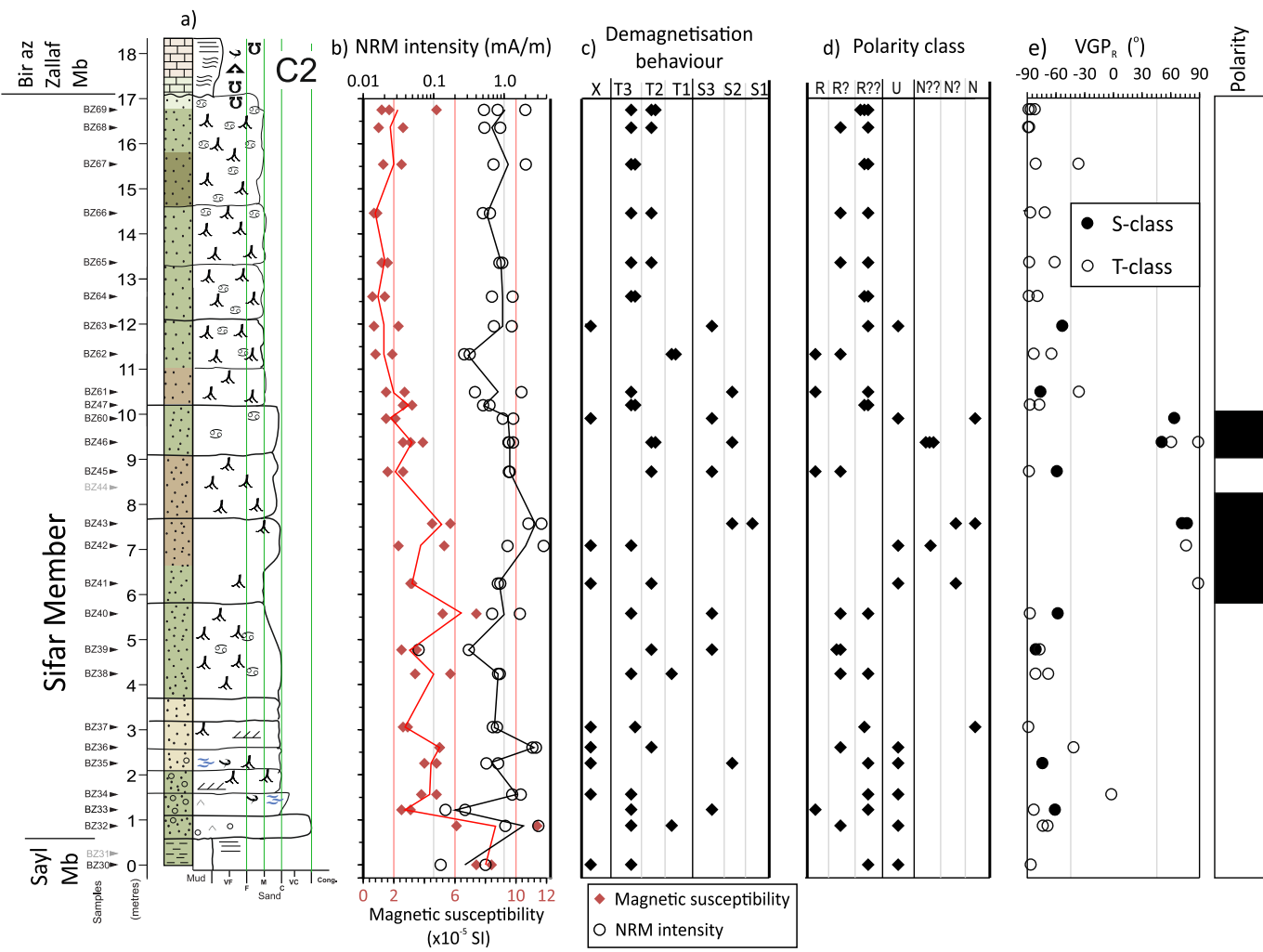


Fig. 9. Magnetostratigraphic data for section SK11. See Fig. 8 for details.

hand column of Table 4). The most tentative magnetozone ZA1r.1n is excluded in correlation options B and C (suggesting that it is spurious) and some short duration normal polarity submagnetochrons in C3B are not detected in options A and B (Table 4; Fig. 13B).

Option A has the greatest similarity to the GPTS, with the largest SMI, PSI and dCor values. This option also has the lowest P_{RV} and P_{dCor} (Table 4), indicating it is the most probable correlation option of the three with a $\geq 99.9\%$ probability of association in both tests. The inclusion of ZA1r.1n in option A suggest that it is a real polarity event (just insufficiently sampled) and that magnetochrons C3Br.1n and C3Br.2n were missed in the lower part of the Sifar Mb again due to insufficiently close sampling spacing (or minor disconformities). This preferred correlation option suggests that the Sifar Mb is late Tortonian to latest Messinian in age with a larger accumulation rate in lower parts of the member. Option A indicates that the Bir az Zallaf Mb C2 and C3 carbonates are early Pliocene (Zanclean) in age (Fig. 13B). The basal ~1 m of the Sayl Mb is of normal polarity in the SK13 section (Fig. 4), a section which is ~10 m below the base of section SK12, which suggests that the base of the Zarzur Fm probably extends into C4n.2n (at c. 8 Ma) in the late Tortonian in Wadi ash Shati (Fig. 13B). Remote sensing data indicate that there is a fourth carbonate in the Bir az Zallaf Mb, with an upper elevation of ~381 m (Fig. 3), so in the Wadi ash Shati area the age of this member extends to a younger level in the Zanclean, perhaps to ~4–4.2 Ma. These relationships suggest the hiatuses at the base and top of the Zarzur Fm have durations of about 3 Myr and 4 Myr, respectively.

7.2. Environmental model for the Zarzur Formation

7.2.1. Carbonate lakes of the Bir az Zallaf Member

Facies C p is the most distinctive in the Zarzur Fm and has rightly attracted the most attention (Geyh and Thiedig, 2008; Abdullah, 2010). Since there are no major hiatus intervals within the C p facies, the facies likely formed in relatively permanent brackish to hypersaline lakes, with minor localised biological and evaporite-related disturbance of the coarse lamination. The abrupt base of these facies, which often overlie sand with abundant rhizoliths (S rt facies), probably indicates a strongly vegetated lake margin, with rapid establishment of carbonate lakes that then expanded over the lake margin sediments (Fig. 15).

Outcrops of the Bir az Zallaf Mb carbonates are elongated and roughly parallel to each other, which we infer to relate to their formation within interdune depressions. Hence, the lacustrine carbonate facies in the Bir az Zallaf Mb likely coexisted with a linear dune system that is best represented by facies S x. Likely parallel with lake formation, adjacent dunes experienced groundwater level variation, supporting plant growth and rhizolith development in adjacent dune sediments, followed by growth of incipient caliche. Hence, facies S rt is interpreted as vegetated dune flanks subjected to frequent water table level changes, leading to partial caliche cementation.

Similar laminated carbonates to those of the Bir az Zallaf Mb in Wadi ash Shati occur at other locations in both the Awbari and Murzuq basins (Drake et al., 2008, 2011). Thiedig et al. (2000) described similar carbonates that they referred to as the ‘Antalkhatá Member’ at an elevation

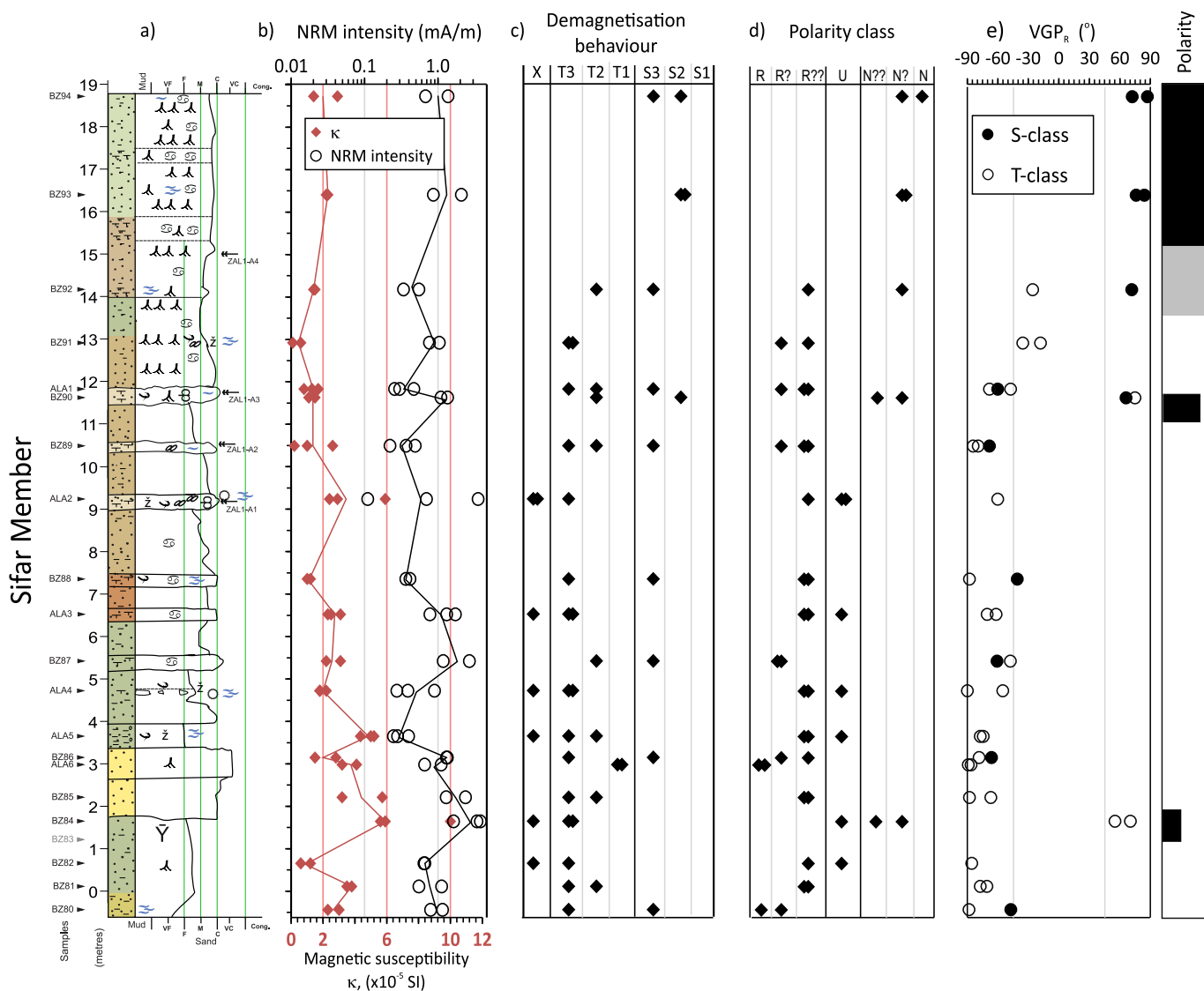


Fig. 10. Magnetostratigraphic data for section SK12. See Fig. 8 for details.

of 500–550 m near Awbari. These have similar $\delta^{18}\text{O}$ - $\delta^{13}\text{C}$ values to samples from Wadi ash Shati (Fig. 14) and may be a much younger carbonate, and/or regional variant of the Zarzur Fm, because it is clear from the data of Hounslow et al. (2017) that the elevation of such units does not necessarily equate to relative age, even if this concept works for Zarzur Fm carbonates locally in Wadi ash Shati. Holocene aged, sometimes stromatolitic carbonates and organic-rich lake sediments are not unusual in interdune depressions in the Awbari Sand Sea (SI Fig. S5I), particularly near the modern groundwater fed lakes such as Lake Mandarah north of Awbari (Burdon and Gonfiantini, 1991; Parker et al., 2008; SI Fig. S5J,K), and within the Murzuq Sand Sea (SI Fig. S5G,H). Hence, it is possible that Bir az Zallaq Mb carbonates may age-transition into modern interdune carbonates within central parts of the Awbari Sand Sea at a variety of elevations.

7.2.2. Siliciclastic environments of the Zarzur Formation

Gastropods, ostracods, foraminifera and ooid-bearing sandstones (facies S og; Table 2), all suggest proximity to lacustrine environments. These lakes likely developed entirely on a sandy substrate or represent marginal fringes to deeper water lakes containing carbonates (Fig. 15). Comparison to modern desert lakes suggests that the ooids were generated in shallow water lake margin settings, where wave agitation is high (Magee et al., 1995). The ooid and bioclast content of facies S og are

like that also seen in facies mS m (samples ALA5 and BZ80; Fig. 4), but more enriched. Hence, the bioclast content in facies S rt and mS m are likely transitional into each other with variable development of additional rhizoliths (Fig. 15).

The S rt. facies is similar to that in the Anthracotheriid Unit in the Megalake Chad successions in northern Chad which bear rich vertebrate faunas (Moussa et al., 2021), and likewise sometimes bear lacustrine diatoms (compare SI Fig. S4D; and Figs. 11, 12 in Moussa et al., 2021). In Megalake Chad the Anthracotheriid Unit was assigned as a perlacustrine facies.

In section SK14 (Fig. 4), gastropod rich facies S og between 5.5 and 9.5 m alternate with possible reworked calcrete mini-nodules (SI Fig. S3d), which represent lake margin deposits with the nodules reworked by wave-action. Lack of a direct transition between the S og and C p facies in any section seen so far indicate that the S og facies formed in a separate type of lake system from the carbonate lakes outlined above. Alternatively, the Bir az Zallaq carbonate lakes developed relatively rapidly (e.g. following prolonged/intense rainfall) without formation of an initial transgressive margin facies.

The more clearly fluvial-related facies are gS and sM. The pebbly character of facies gS suggests deposition in a fluvial environment with sufficient flow to transport rounded pebbles. In comparable facies to sM in modern arid settings (Rust and Nanson, 1989; Magee et al., 1995) the

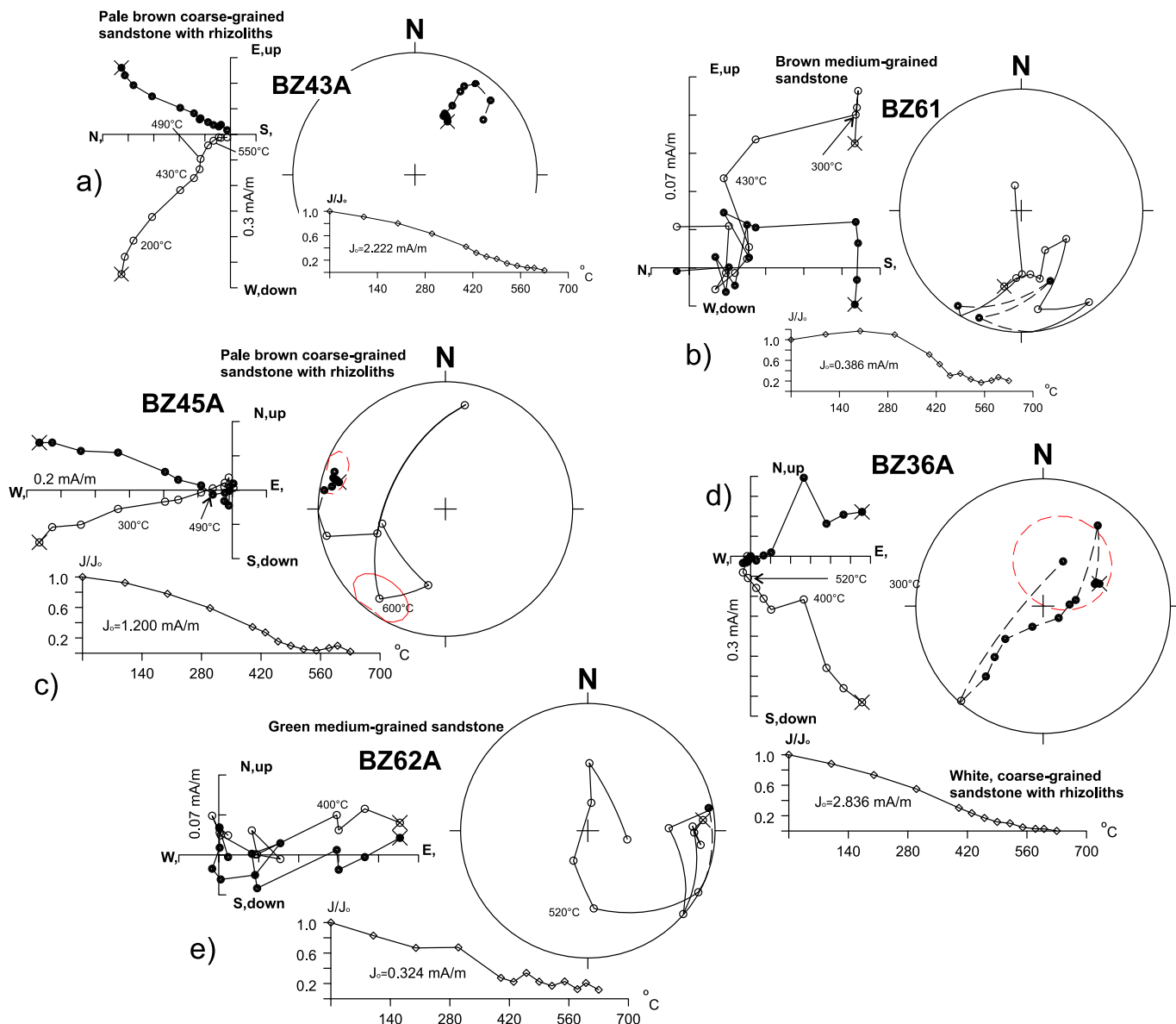


Fig. 11. Demagnetisation data for representative specimens (specimen name in bold). For each is shown a Zijderveld (1967) plot, a stereographic projection and a normalised intensity decay plot. All directional plots in stratigraphic coordinates. Scale on Zijderveld plot axis is the magnetisation between ticks. Natural remanent magnetization (NRM) intensity (J_0) and NRM step marked with X. In the following text the demagnetisation class, polarity classification and other extracted components shown inside (..), ρ = excess standard deviation, the ‘fitting parameter’ used in LINEFIND expressing the degree of relaxation of model measurement variances. ChRM = characteristic remanent magnetisation, GC = great circle. LT, MT = low and mid stability components, respectively. Specimens lithology is marked on the plots. Measurement points in c) and d) with larger than usual γ_{95} measurement confidence cone are shown in red. A) BZ43A: section SK11, 7.57 m (S1, N), with ChRM 490–550°C (028°, 52°, $\alpha_{95} = 7^\circ$, $\rho = 1.7$), with MT component 200–430°C (026°, 44°, $\alpha_{95} = 4^\circ$). B) BZ61: Section SK12, 10.49 m (S2, R), with ChRM component 300–430°C (191°, –34°, $\alpha_{95} = 15^\circ$, $\rho = 1.2$) and LT component NRM–300°C (271°, 29°, $\alpha_{95} = 31^\circ$). C) BZ45A: from section SK11 at 8.72 m, (S3, R). Strong composite initial directions with isolation of southerly negative inclination component. ChRM 600°C to origin (222°, –48°, $\alpha_{95} = 30^\circ$, $\rho = 2.0$) with MT component 300–490°C (293°, +16°, $\alpha_{95} = 9^\circ$). D) BZ36A: section SK11 at 2.61 m (T2, R?). Strong GC trend to south from probable Brunhes overprint in initial steps. ChRM GC plane NRM to origin (140°, –10°, $\alpha_{95} = 6^\circ$, $\rho = 2$) and LT component NRM to 400°C (062°, 43°, $\alpha_{95} = 7^\circ$) and MT component 520–600°C (237°, 71°, $\alpha_{95} = 5^\circ$). E) BZ62A: section SK12 at 11.33 m (T1, R). Partial recovery of southerly reverse, after initial steps with a composite easterly direction. ChRM GC fit 520°C to origin (091°, 2°, $\alpha_{95} = 18^\circ$, $\rho = 3$), with LT component NRM to 400°C (072°, 18°, $\alpha_{95} = 12^\circ$) and MT component 520–600°C (182°, 1°, $\alpha_{95} = 18^\circ$). Further examples are shown in SI Fig. S11. (For interpretation of the references to colour in this figure legend, the reader is referred to the web version of this article.)

pelletised mud-rich facies is a fluvially transported sand-sized mud aggregate, with an admixture of minor quartz sand. Also, samples from facies SM are particularly sensitive to wetting, and are probably rich in expandable clays, as in comparable modern settings. Mudstones of comparable age from the Megalake Chad Basin are also rich in smectite, derived from reworking of vertisols (Moussa et al., 2016).

Massive sandstone facies S m may result either from a lack of original depositional structure, or from the original structure having been

destroyed by biological or physical processes. This facies is more common in the lower part of the Sifar Mb, suggesting that it may be transitional between more fluvially-impacted units low in the Sifar Mb and the fluvial dominance in the Sayl Mb. The environment could be interpreted in either of the following two ways:

- 1) A sandy playa facies, in which aeolian sand was trapped on damp surfaces in interdune depressions and vegetated lake margin

Table 3

Palaeomagnetic directional means for the Zarzur Fm (stratigraphic coordinates), reversal tests and VGP poles.

Type/ fm	Dec. (°)	Inc. (°)	k/ α_{95} (°)	Ns/Nl/Np	Reversal Test	G_0/G_C (°)	Plat./ Plong. (°)	Dp/Dm (°)	A95 (min, max), %VGP ₄₅
Zarzur Formation									
Specimen line fits [§]	10.4	46.8	11.7/6.5	45/45/0	Rc	8.3/13.7	80.8/98.3	5.4/8.4	–
Sample mean ⁺	6.2	50.8	11.4/7.9	32/45/22	Rc	5.9/16	83.2/65.8	7.2/10.7	9.6 (3.0,13.1),15.6

⁺ Using T-class specimens and the method of McFadden and McElhinny (1988) for samples with only one or more S-class specimens. [§] = conventional Fisher mean using specimen S-class data. Ns = number of specimens for specimen mean and number of samples for sample mean, Nl = number of specimens used with fitted lines, and Np = number of specimens with great circle planes used to determine the mean direction. α_{95} , Fisher 95 % cone of confidence, k, Fisher precision parameter. G_0 is the angular separation between inverted reverse and normal polarity directions, and G_C is the critical value for the reversal test (McFadden and McElhinny, 1990). Both reversal tests use the common K value test. Plat. and Plong. are the latitude and longitude of the mean virtual geomagnetic pole. A95 (min, max) = Fisher 95 % confidence interval for VGP-based site mean (N_s sites), and A95_{min} and A95_{max} are threshold values of Deenen et al. (2014). %VGP₄₅ = percent of samples yielding VGP latitude < |45°|, as a reflection of the match to the modern geocentric dipole field models and palaeomagnetic data in which %VGP₄₅ is ~3–4 % (Cromwell et al., 2018). Statistics were determined using Palaeomagtool v.5 (Hounslow, 2023b).

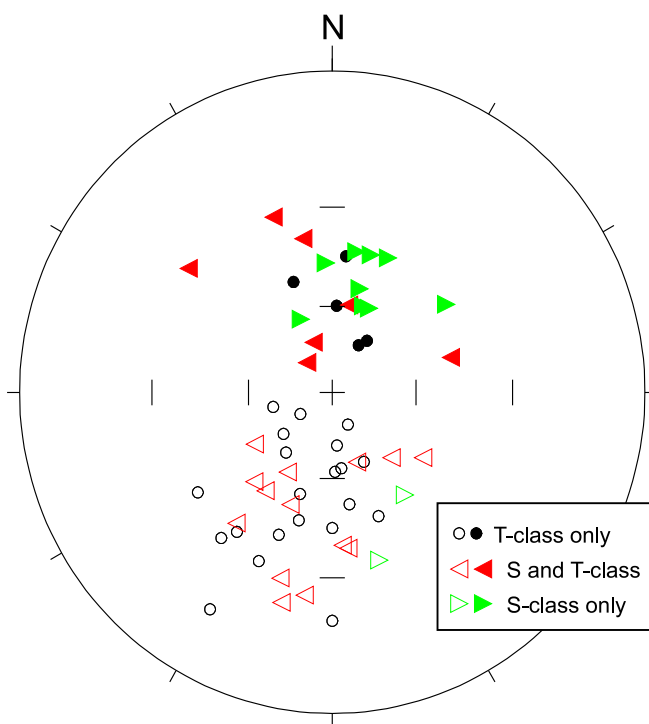


Fig. 12. Stereographic projections of sample mean ChRM directions (see Table 3 for overall mean directions and SI Fig. S13 for other component directions).

deposits. Mudcracks in section SK12 are consistent with this (SI Fig. S3e). Such sandy playas are common in the modern Libyan Sahara with flat hard sand surfaces often covered with adhesion ripples (SI Figs. S5d–f). Abotalib et al. (2016) referred to these as type II playas, which lack carbonate, chemical precipitates and the pustulated surfaces commonly found in halite and gypsum-bearing playas. Haynes Jr. (2001) described similar Holocene playa sediments from the Darb el Arba'in Desert (Egypt and Sudan), and Magee et al. (1995) from Lake Eyre (Australia), where they are sometimes associated with ooids (i.e. transitional toward facies mS m).

2) Aeolian sand-sheets that have become stabilised and subsequently undergone intense rootlet development and burrowing to destroy original aeolian lamination, which Haynes Jr. (2001) referred to as stage 3 pedogenesis in the Selima Sand Sheet (Egypt-Sudan border). Both these environments may have existed in the Zarzur Fm (Fig. 15).

Aeolian cross-bedded facies S x is uncommon in the Zarzur Fm in Wadi ash Shati but is present in the lower parts of the formation in

sections SK10 and SK14 (Fig. 4; SI Fig. S2d). This perhaps relates in part to the poor preservation potential of this facies because the weakly consolidated aeolian sandstones are readily reworked by modern desert erosion. In contrast, the more cohesive and consolidated lake and calcrite-bearing sediments are less easily reworked, with carbonate units commonly forming protective, but wind-eroded surfaces when exposed in the modern desert. Thus, modern erosion of Zarzur Fm dune sediments (Fig. 7B) has preferentially preserved the carbonate-enriched inter-dune sediments and biased the current outcrop pattern toward inter-dune sediments. Consistent orientation of the ancient and modern linear dune systems suggests that the wind regimes were similar in both cases. Moussa et al. (2021) has also inferred the similarity of directional wind-regimes between late Miocene and modern aeolian dunes in the Djourab Desert, northern Chad.

7.2.3. Modern analogues

The Bir az Zallaq Mb carbonates possess coarse lamination, associated in some locations with primary gypsum, bedding disruption (teepees, etc.) and high primary dolomite contents. This suggests that a suitable modern analogue is the Holocene dolomite-bearing Coorang-type saline lakes (e.g. Salt Creek lakes; Warren, 1990). A vital element of the Coorang dolomite-rich lakes is that they are fed by Mg-rich and Ca-rich groundwater under substantial evaporitic losses (James and Bone, 2022). A similar situation may have prevailed for the Bir az Zallaq Mb carbonates.

Perhaps the best modern analogue for comparable compound siliciclastic and carbonate dominated lake systems are the Ounianga Lakes of northern Chad which have varied salinity due to differing inflow and outflow conditions, lake volume and evaporitic losses (Van Bocelaer et al., 2011). The Ounianga Lakes have various substrates from coarse sand in Lake Boku and sandy mud in Lake Girki, to lakes with fine-grained carbonates with variable organic matter content (Lakes Edem, Djara, Hogou, Agouta; Van Bocelaer et al., 2011; Creutz et al., 2016). In the Zarzur Fm, muddy organic rich lake facies have not been seen in outcrop; instead, the muddier facies are related to fluvial transport systems lower in the Zarzur Fm. Lake Boku may be a suitable analogue for the S og facies, since *M. tuberculata* in the modern Ounianga lakes is limited to that lake (Creutz et al., 2016). Deposits of Lake Hogou at Ounianga may be a comparable analogue for the Bir az Zallaq Mb carbonates, although there the carbonate is calcite (Creutz et al., 2016). These possible analogue lakes are shallow (5–13 m deep), with fresh to brackish water derived from the Nubian Sandstone aquifer. Correlation of the C1 carbonate from section SK15 to SK14 (Fig. 4) implies that local carbonate lake systems coexisted with clastic-substrate lake systems in adjacent interdune corridors as in the Ounianga Lakes.

The vegetated lake margins are likely represented by the abundant rhizolith-bearing facies in the sections (Fig. 15), particularly if these contain ostracod and gastropod shells (as in section SK14), whereas the absence of shell material in facies S rt in sections SK11 and SK12 suggests the vegetation probably also utilised groundwater and was more distant from lake margins, outside the limits of local reworking of

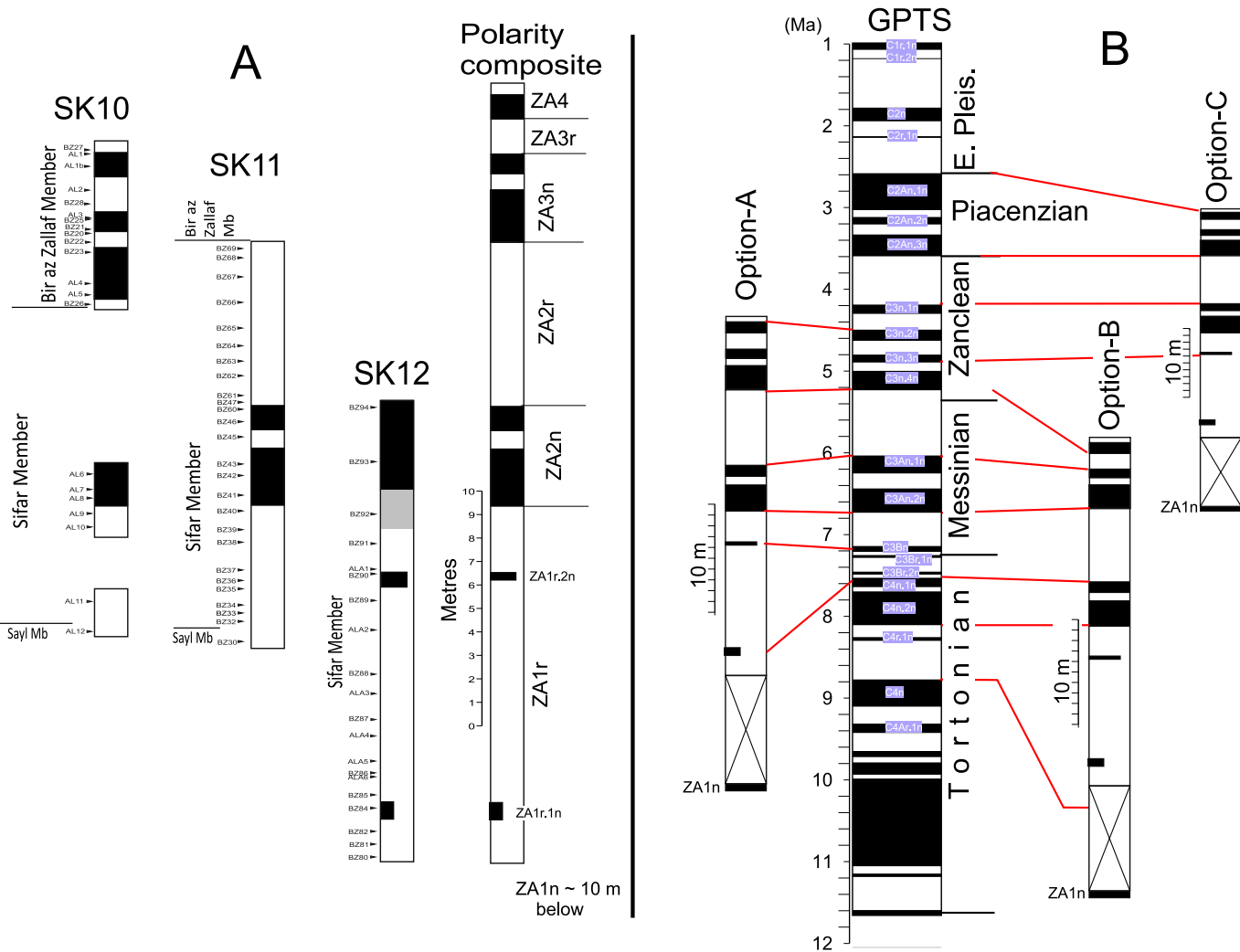


Fig. 13. A) Construction of a composite magnetostratigraphy using data from the three studied sections. Magnetozone ZA2n is evident in all three sections and allows these sections to be correlated. All use the same height metre scale. B) Correlation options for the Zarzur Fm composite to the geomagnetic polarity timescale (GPTS) of Ogg (2020). Selected normal polarity magnetochrons are labelled. See Table 4 for statistics for these comparisons. Correlation option A is the preferred one.

lacustrine faunas. In the modern Ounianga lakes, the vegetated margin can stretch for several hundred meters from the lake shore which is often less than 10 m wide. Facies with abundant rhizoliths tend to be more frequent in the upper parts of the Sifar Mb, which suggests that groundwater availability increased upward in the succession.

The absence of evidence for shoreline deposits has been used as a primary means to reject the idea of a wetter and green Late Pleistocene Fezzan Basin (Quade et al., 2018). However, this work indicates that a more nuanced view of likely environmental conditions is needed, such that a green central Sahara during the latest Tortonian and Early Pliocene may have existed as an extensive patchwork of inter-dune lakes that may have covered the Fezzan megalake basin, an area that is now occupied by the Awbari and Murzuq sand seas.

7.3. Palaeohydrology of the Zarzur Formation lakes

Covariant trends in $\delta^{18}\text{O}$ – $\delta^{13}\text{C}_{\text{carb}}$ are typical of primary lacustrine carbonate from hydrologically closed basins and represent increasing evaporation or residence time of source waters (Talbot, 1990; Li and Ku, 1997; Leng and Marshall, 2004; Horton et al., 2016). The least evolved, and most negative part of the trends, represent conditions that are closest to the source water, which implies that data cluster ④ and those in the groundwater cements groups should be closest to the least evolved water (Fig. 14). Conversely, the most evolved waters with higher salinity

are those with larger $\delta^{18}\text{O}$ and $\delta^{13}\text{C}_{\text{carb}}$ like those of data cluster ①. The larger $\delta^{18}\text{O}$ values in both trends reflect preferential evaporative ^{16}O loss (Leng and Marshall, 2004). The comparable range of isotopic values for both the Aqar Mb and Zarzur Fm suggests that the formations share similar water sources and sets of environmental controls. A likely interpretation is that the two covariant trends reflect different kinds of water sources: a) riverine/fluvial and b) groundwater sources.

- The isotopic sample group ④ (Fig. 14) reflects a lower salinity (oligohaline) source as demonstrated by its faunal content (Gaven et al., 1981; Rosso and Gaillard, 1982; Petit-Maire, 1989, 1994) and its position close to a river delta (Drake et al., 2018). The faunal content in the Shati Fm associated with this group is typical of modern lake Chad (Rosso and Gaillard, 1982), a fresh-water lake (Bouchez et al., 2016). Trends 2 and 3 share the least evolved water characteristics, with the low $\delta^{18}\text{O}$ and $\delta^{13}\text{C}_{\text{carb}}$ representing the least evolved end of this riverine source.
- For the middle and upper parts of the Zarzur Fm, the environmental model suggests linearly oriented lacustrine systems bounded by dunes, where water transfer into the interdune basins was only feasible via groundwater or rainfall. The groundwater cements cluster (Fig. 14a) corresponds to a lower salinity system which is borne out by its association with charophyte remains in the Zarzur Fm (Fig. 4). Such remains are characteristic of low salinity waters in

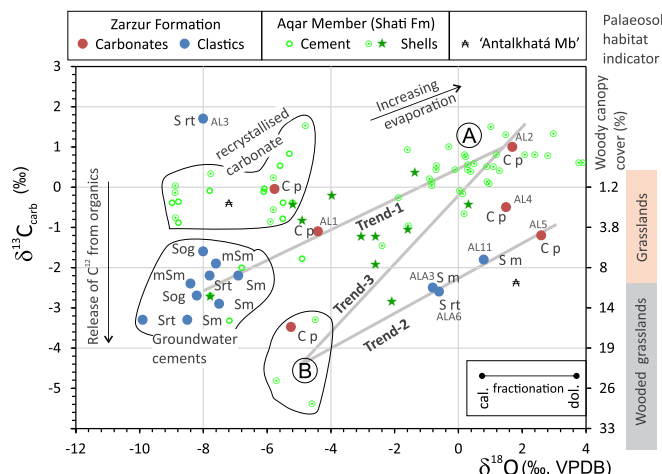


Fig. 14. Stable carbon isotope data for the Zarzur Fm and Aqar Mb (from Gaven et al., 1981) of the Shati Fm. Stars are Aqar Mb data from Geyh and Thiedig (2008) (their Fig. 14), probably mostly from shell material although some (not specified) are from whole-rock samples, which may account for some of their data falling in and near the recrystallised carbonate field. Differences to Aqar Fm data from Gaven et al. (1981) may relate to local, outcrop-related differences in hydrology. Samples are labelled with facies codes (Table 2) and others sample codes as follows: C p code, or ⚡ (but no sample codes) are Bir az Zallaq Mb carbonates or the Antalkhatá Member of Geyh and Thiedig (2008), respectively. The fractionation line is the $\delta^{18}\text{O}$ difference between dolomite and calcite fractionation. Wood canopy cover % from Cerling et al. (2011).

North African Holocene and Late Pleistocene sediments, including the northerly central part of Palaeolake Shati ($\sim 27^{\circ}29', 26^{\circ}N$; $14.0^{\circ}E$; Fig. 3; Soulié-Märsche, 2008). Its association with *M. tuberculata* (which is primarily an oligohaline species), which can tolerate temporary salinity up to $\sim 25\%$ (Rosso and Gaillard, 1982; Kowalek, 2006) also points to low salinity waters. The modern aquifer of the Qarqaf High is near the surface in Wadi ash Shati and is artesian and has been persistently used for irrigation since early human occupation (Whitcomb, 1957; Merlo et al., 2013). Hence, the Qarqaf High was likely a major artesian groundwater source during the deposition of the Zarzur and Shati formations. Petit-Maire (1989, 1994) and Drake et al. (2018) have also suggested substantial groundwater contributions for this and other Late Pleistocene lakes in the Fezzan.

For trends 1 and 2, the difference in the least-evolved $\delta^{13}\text{C}_{\text{carb}}$ end-member values likely relate to greater plant and soil respiration, which is a significant control on soil $\delta^{13}\text{C}$ (Sheldon and Tabor, 2009). The 2‰ to 3‰ offset in $\delta^{13}\text{C}_{\text{carb}}$ between these trends is typical of the offset in modern east African soil carbonate, with the larger $\delta^{13}\text{C}_{\text{carb}}$ values more typical of grassland soils and the smaller values typical of woodlands (Cerling, 1992; Tipple and Pagani, 2007). Cerling et al. (2011) quantified such differences in east African palaeosols as the

proportion of woody cover, calibrated against modern soils. Hence, the low $\delta^{13}\text{C}_{\text{carb}}$ end of Trend-2 represents $\sim 10\%$ more woody cover compared to the groundwater group of Trend-1 (right hand scale of Fig. 14).

Intermediate isotopic values in these trends represent either: a) middle stages in evaporation or residence time of these waters in the respective trends, in lakes of variable lake level (but vertically well mixed waters), or b) spatial variation of waters with differing evolutive state and laterally poorly mixed lake water. The latter option is represented by Trend-3 where the ⚡ and ⚡ groups (formed from samples of the Aqar Mb) represent different geographic positions in Palaeolake Shati that had differing salinities. The limited number of intermediate values on Trend-3, but many in the most-evolved (and higher salinity) end of this trend, suggest a relatively stable hydrological balance in Palaeolake Shati over several thousand years. A comparable analog for Palaeolake Shati may be modern Lake Chad, where near the inflow $\delta^{18}\text{O}$ is lower by $\sim 8\%$ compared to the most evolved, and highest salinity parts of the lake (Bouchez et al., 2016). A comparable effect could have impacted the lake systems of the Zarzur Fm, although the smaller lake size (as suggested by the environmental model) may have suppressed this spatial variation. The large $\delta^{18}\text{O}$ range in both the Aqar and Zarzur Fm suggests small to medium sized lakes for both cases (the Aqar Mb lake had an area of $\sim 1700 \text{ km}^2$; Drake et al., 2018) as does the size of the interdune depressions that the carbonates of the Zarzur Fm appear to represent (Fig. 7B).

An important unknown about the Zarzur Fm isotopic data is the carbonate species of the samples, which were not measured directly. Hence, part of the $\delta^{18}\text{O}$ variation could relate to fractionation differences between calcite and dolomite of $\sim 3\%$ in $\delta^{18}\text{O}$ (Leng and Marshall, 2004). However, this is smaller than the $\sim 8\%$ difference between siliciclastic-rich samples in Trend-1 and Trend-2, and the $\sim 7\%$ difference in the C p facies samples grouped at $\sim -5\%$ and 2% in $\delta^{18}\text{O}$, which indicates that the carbonate species may have had a limited impact.

With the sparse isotopic dataset from the Zarzur Fm and lack of details on stratigraphic changes, these interpretations are open to more detailed cm/dm scale study on the Bir az Zallaq Mb carbonates, which should yield a better understanding of any spatial and time-varying hydrological balance of the C1 to C4 carbonates.

7.4. Palaeorainfall in the Fezzan: observations and models

Northward intrusion of African monsoon (summertime) rainfall has been the pre-eminent explanation for greening of the Sahara during humid episodes since 8 Ma (Larrasoña et al., 2013; Tierney et al., 2017; Wu et al., 2017; Larrasoña, 2021), including in the Fezzan (Drake et al., 2018). However, it is an open question if this is the case for all the Sahara north of the central Saharan watershed (represented by the $>800 \text{ m}$ elevations of the Hoggar and Tibesti Massifs), as also noted by Tzedakis (2007) and Herold and Lohmann (2009) and discussed by Cheddadi et al. (2021) and Couper et al. (2025). Modern precipitation on the north African coast is mostly from westerly cyclonic systems with moisture originating from the Atlantic or Mediterranean during the autumn and

Table 4
Statistics for magnetostratigraphic correlation models to the GPTS.

Correlation model	SMI, PSI, dCor	P _{RV} , P _{dCor}	Nc	Absent/ extra magnetozones
Option-A	0.742, 0.877, 0.850	0.0001, 0.001	13	C3Br.1n, C3Br.2n/none
Option-B	0.621, 0.755, 0.745	0.001, 0.009	11	C3Bn, C3Br.1n, C3Br.2n /ZA1r.1n
Option-C	0.525, 0.647, 0.665	0.09, 0.665	10	none/ ZA1r.1n

SMI, PSI = similarity of matrices index and Procrustes similarity index (Indahl et al., 2018), and dCor = distance correlation (Székely and Rizzo, 2017), all with ranges 0–1.0 (none to perfect similarity), P_{RV} = the RV-based statistic testing the probability of association between the sets as in Josse and Holmes (2016), and P_{dCor} the probability of correlation using the dCor statistic. Nc = number of magnetozones/chrons in the comparison. Absent/extra = normal polarity magnetozones: absent from the reference GPTS set used/ additional normal magnetozones in the comparison set. In each correlation model the thickness of Zarzur Fm magnetozones were scaled to Ma, using the upper and lower correlation points to the GPTS (as in Fig. 13b). These inferred durations (in Ma) were used as t₀, t₊₁ and t₋₁ (see SI for datasets). Magnetochron ages are from Ogg (2020).

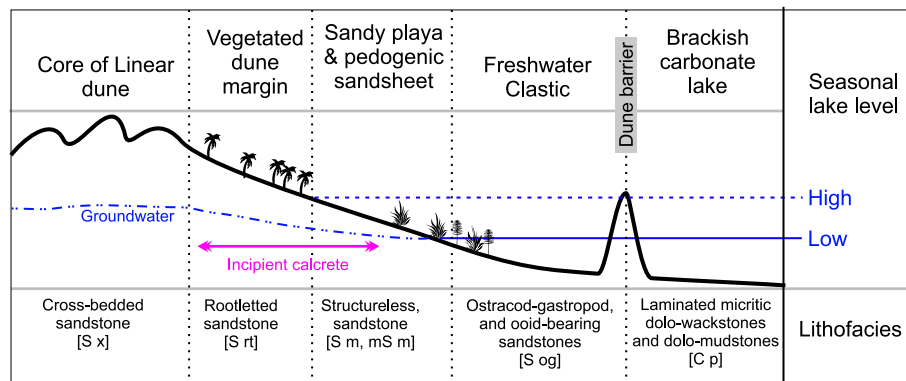


Fig. 15. Environmental facies model for the Zarzur Fm, with corresponding facies codes. The brackish lake environment applies only to the Bir az Zallaf Mb. See text for details.

winter (Zhao et al., 2012; Armon et al., 2024; Givon et al., 2024), hence this region is not inferred to be under monsoonal influence since at least 8 Ma (Zhao et al., 2012; Marzocchi et al., 2019). The Fezzan region falls in the transition zone whereby perhaps both monsoonal and/or westerly sourced cyclonic rainfall could have potentially occurred (Edmunds et al., 2004). If modern Saharan precipitation events are a guide to the complexity of ancient rainfall patterns, then palaeolatitude is an

imprecise guide to moisture source. For example, modern rainfall in southern Algeria, at a similar latitude to the Fezzan is much more strongly impacted by summer storms than in the Fezzan, which is protected from southerly summer sources by the Hoggar and Tibesti Mountains (Armon et al., 2024, their Fig. 7).

Several strands of evidence can be used to infer rainfall sources during Saharan humid intervals, drawing mostly on assessments from

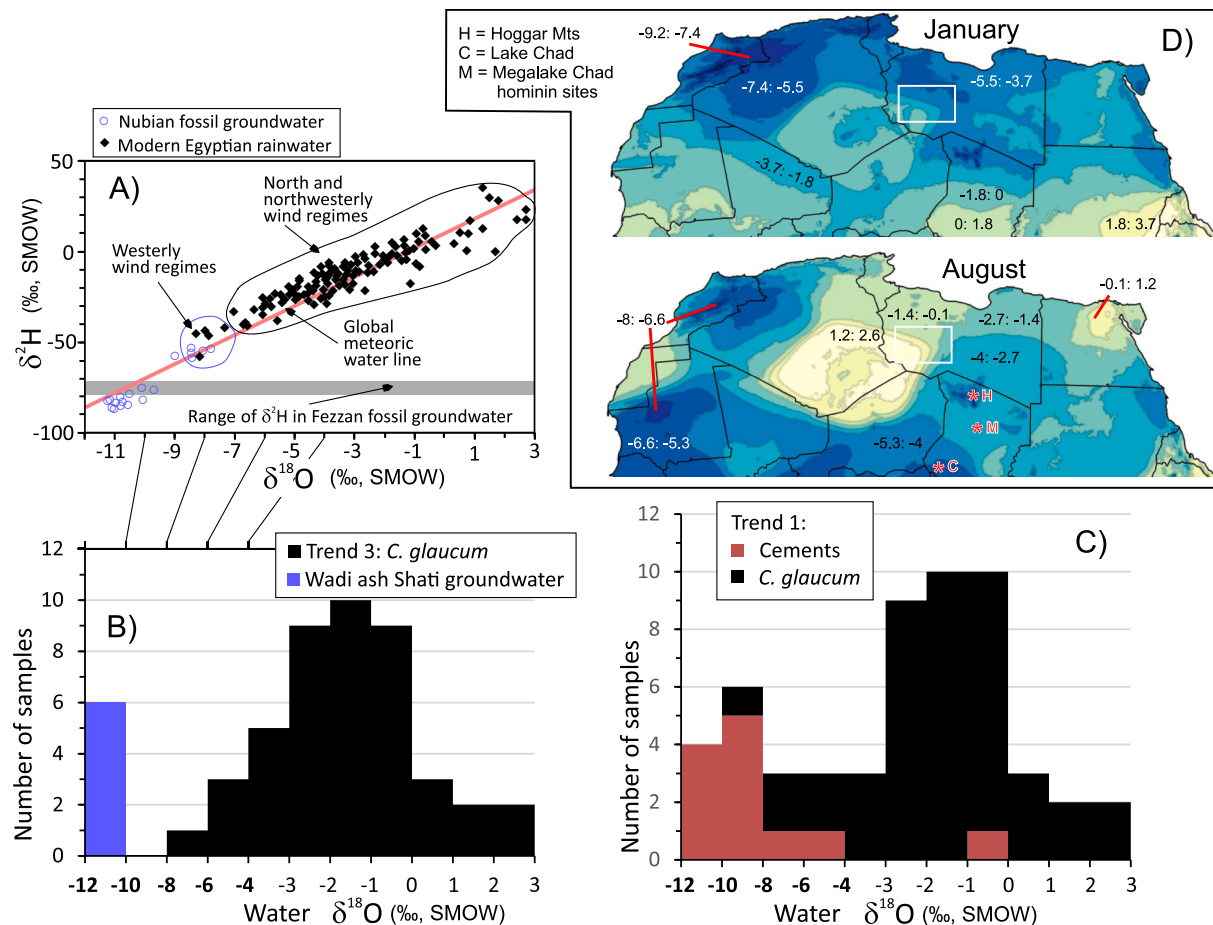


Fig. 16. A) Egyptian rainfall and groundwater isotopic compositions from Abouelmagd et al. (2012) divided to corresponding values in B). Range of $\delta^2\text{H}$ values in Wadi ash Shati groundwaters from Salem et al. (1980). B), C) $\delta^{18}\text{O}_{\text{SMOW}}$ values of equilibrium water sources for *C. glaucum* from the Aqar Mb (in black) and Zarzur Fm (in red) samples, subdivided according to covariance trends 1 and 3 in Fig. 14. Groundwater values from Wadi ash Shati (in blue) from Salem et al. (1980). See text for conversions used. In each, $\delta^{18}\text{O}_{\text{SMOW}}$ values are binned into two differently scaled linear segments, marked as bold and non-bold. D) Modern average January and August precipitation $\delta^{18}\text{O}_{\text{SMOW}}$ over the Sahara (from Waterisotopes.org, 2025), with $\delta^{18}\text{O}_{\text{SMOW}}$ ranges indicated for the corresponding coloured regions. The white box marks the Fezzan study area as in Fig. 1. (For interpretation of the references to colour in this figure legend, the reader is referred to the web version of this article.)

the wider north Africa. These are: a) fossil groundwaters (Joseph et al., 1992; Fontes et al., 1993; Jasechko, 2016), b) fossil flora and fauna (Kindermann et al., 2006), c) $\delta^{18}\text{O}$ data from carbonates (Bar-Matthews et al., 2003; Prendergast et al., 2015; Horton et al., 2016), d) modern analogue lake systems (Bouchez et al., 2016; Rieder et al., 2025) and e) numerical climatic models (Kutzbach et al., 2014; Gierz et al., 2017; Tierney et al., 2017). Each source is discussed separately below.

7.4.1. Fossil groundwaters

The deep groundwater systems of the central Sahara are dominated by fossil water accumulated during more humid intervals of the late Quaternary. Its composition is largely thought to reflect a long-term average of rainfall recharge during wetter intervals (Jasechko, 2016; Dodo and Zuppi, 1997; Beyerle et al., 2003; Joseph et al., 1990). As a result of effective recharge mechanisms, groundwater is likely to mostly reflect heavier rainfall events (Goni et al., 2001; Beyerle et al., 2003; Edmunds et al., 2004; Jiang et al., 2024), which likely matched events recharging Saharan palaeolakes. Areas north of the central Saharan watershed have groundwaters with increasing ‘continentality’ (Rozanski et al., 1993) to the east with $\delta^{18}\text{O}$ and $\delta^2\text{H}$ reflecting progressive water vapour condensation from westerly derived storms (Sonntag et al., 1980; Sultan et al., 1997). This results in lower $\delta^{18}\text{O}$ with increasing continentality (Joseph et al., 1992; Rozanski et al., 1993; Abouelmagd et al., 2012). This demonstrates the former more southerly position of the rainfall regimes typical of modern northern Libya, which may have remained dominated by Mediterranean winter-storms (Reade et al., 2016; Givon et al., 2024). However, in the Egyptian Western Desert $\delta^2\text{H}$ values from ^{81}Kr -dated groundwater sourced from recharge areas in SW Egypt, indicate a dominant Atlantic moisture source during the last 1 Myr and unlike the Mediterranean moisture sources, as at present (Sturchio et al., 2004); a feature consistent with the continentality effect. Late Pleistocene groundwaters from Wadi ash Shati (Salem et al., 1980) and Holocene speleothems in the NE Sahara (El-Shenawy et al., 2018) consistently suggest palaeorainfall causing recharge in Libya and western Egypt likely had $\delta^{18}\text{O}_{\text{SMOW}}$ of about $-11\text{\textperthousand}$ to $-10\text{\textperthousand}$ (Edmunds et al., 2004; Fig. 16A, B).

South of the Central Saharan watershed in the Sahel (at $\sim 14^\circ\text{N}$), the rainfall continentality effect increases to the west, giving lower $\delta^{18}\text{O}_{\text{SMOW}}$ to the west (Joseph et al., 1992; Andrews, 1993), representing a fossil groundwater regime impacted by summer monsoonal rainfall (Joseph et al., 1992; Gasse, 2000; Beyerle et al., 2003). At latitudes ~ 10 – 13°N fossil groundwater suggests the palaeometeoric supply for Megalake Chad had mean $\delta^{18}\text{O}_{\text{SMOW}}$ of $-6 \pm 0.6\text{\textperthousand}$ (Maduabuchi et al., 2006). Further north (~ 17 – 22°N), but a little to the south of the central Saharan watershed, fossil groundwaters have depleted $\delta^{18}\text{O}_{\text{SMOW}}$ of $-10\text{\textperthousand}$ to $-11\text{\textperthousand}$, much like that from the Fezzan (Salem et al., 1980; Fontes et al., 1993; Joseph et al., 1990; Dodo and Zuppi, 1997). These low $\delta^{18}\text{O}$ values may either be caused by enhanced convection, the so called ‘amount’ effect (Fontes et al., 1993), and/or represent recharge from the higher elevation flanks of the central Saharan watershed (Dodo and Zuppi, 1997). This latter process is the altitude effect (Rozanski et al., 1993; Pape et al., 2010). Both processes result from preferential removal of the heavier isotope during condensation processes (Rozanski et al., 1993). Hence, fossil groundwaters have similar low $\delta^{18}\text{O}$ both north and south of the central Saharan watershed, without substantive evidence of westward increasing continentality in fossil groundwater signatures north or immediately south of the watershed, neither having higher $\delta^{18}\text{O}$ like that seen in monsoon-impacted systems farther south.

7.4.2. Palaeontological indicators of season

In contrast to the long-term average of meteoric water expressed in groundwater, palaeobotanical data provide evidence of the principal rainfall season. In the Egyptian Western Desert ($\sim 25^\circ\text{N}$), Holocene sediments record *Anastatica hierochuntica* (the Jericho rose), which is a good indicator of a winter rainfall season, a species found in Egyptian Holocene deposits as far south as about $\sim 23.7^\circ\text{N}$ (Kindermann et al.,

2006), and currently restricted to regions with mean annual precipitation of ~ 25 – 80 mm , which is more typical of modern north African coastal regions. Also, in Morocco, the African Humid Period (ca. 14.5–5 ka) was an interval of enhanced winter rainfall as seen in pollen records (Cheddadi et al., 2021).

South of the central Sharan watershed the land snail *Limicokaria kambeul chudeaui* points to Sahelian forest or forest-savanna biomes in the mid Holocene at $\sim 17.5^\circ\text{N}$ in Niger, Chad and Sudan (Haynes Jr. and Mead, 1987), and by association a summer monsoon season. The limit of this land snail points to rainfall conditions of $\sim \leq 300\text{ mm/yr}$ north of this latitude, which is comparable to pollen-based evaluations which indicate a steep northward moisture loss into true desert by $\sim 19^\circ\text{N}$ in NW Sudan (Ritchie and Haynes, 1987).

7.4.3. Source water $\delta^{18}\text{O}$ compositions

To compare the carbonate $\delta^{18}\text{O}_{\text{carb}}$ from the Zarzur and Shati formations with possible host waters (in $\delta^{18}\text{O}_{\text{SMOW}}$) we used:

- a) The relationship of Borówka et al. (2012) for the *C. glaucum*, where near isotopic equilibrium occurs for carbonate growth (Mook, 1971; Borówka et al., 2012),
- b) The isotopic equilibrium relationship of Leng and Marshall (2004) and applied to the Zarzur Fm carbonates at 23°C (Fig. 16b, c) using $T^\circ\text{C} = 13.8 - 4.58(\delta^{18}\text{O}_{\text{carb}} - \delta^{18}\text{O}_{\text{SMOW}}) + 0.08(\delta^{18}\text{O}_{\text{carb}} - \delta^{18}\text{O}_{\text{SMOW}})^2$. Near isotopic equilibrium in the Zarzur Fm carbonate cements is assumed following studies on pedogenic carbonates by Breecker et al. (2009), who showed a seasonal bias to soil water conditions during the dry season (hence more groundwater influence), when carbonate growth preferentially occurred.

The least evolved $\delta^{18}\text{O}_{\text{carb}}$ values are likely to represent values closest to source waters. In this respect the *C. glaucum* $\delta^{18}\text{O}_{\text{carb}}$ values in Group @ (Fig. 14) suggest formation waters were ~ 3 – 5\textperthousand more evolved (corresponding to three samples with $\delta^{18}\text{O}_{\text{SMOW}}$ of $-7.1\text{\textperthousand}$ to $-5.9\text{\textperthousand}$ in Fig. 16B) than Wadi ash Shati groundwater (blue column in Fig. 16B). In contrast groundwater cement values have a substantial fraction that are similar to modern groundwaters, but still with ~ 2 – 3\textperthousand increase in evolution in many samples (cements in Fig. 16C). This additional evolution in formation waters in either case could be due to additional evaporation, or a riverine water source more evolved in $\delta^{18}\text{O}_{\text{SMOW}}$ than the modern fossil groundwater. This latter possibility could relate to: 1) a more southerly riverine input, perhaps with a stronger Sahelian isotopic signature, or 2) a larger $\delta^{18}\text{O}_{\text{SMOW}}$ of the moisture compared to that which recharged the groundwaters.

Seasonality has a large impact on present day average $\delta^{18}\text{O}$ of precipitation (Bowen et al., 2005), with lower $\delta^{18}\text{O}$ focussed in the winter months in Libya (Fig. 16d). Abouelmagd et al. (2012) demonstrated using modern storm tracks that rare westerly-derived rainfall events (in Egypt) with $\delta^{18}\text{O}$ of $\sim -8.5\text{\textperthousand}$ to $-7\text{\textperthousand}$ do occur on the modern NE African coast with some overlap in $\delta^{18}\text{O}$ and $\delta^2\text{H}$ values to fossil groundwaters (Fig. 16A). These westerly-derived events could be representative of groundwaters that flowed into Palaeolake Shati, and by association possible rainwater and riverine inputs to Zarzur Fm lakes. This Egyptian–Libyan comparison seems valid since fossil groundwaters in Fezzan have similar $\delta^2\text{H}$ values to those of fossil groundwaters of the Egyptian Western Desert (Fig. 16A; Abouelmagd et al., 2012; Abotalib et al., 2016), although clearly there is important modern regional variation in average $\delta^{18}\text{O}$ values (Fig. 16d). Consequently, a viable model for the rainfall systems of the Shati and Zarzur Fm lakes is that waters may have been derived from westerly-derived extreme events, much like the dominant rainfall pattern in the present day hyperarid parts of Libya and Egypt (Armon et al., 2024), but with a greater annual precipitation.

7.4.4. Lake filling episodes and modern hydrological analogues

A challenge concerning Saharan megalakes has been to understand the rainfall and atmospheric circulation conditions that allowed lake

filling. Simple mean annual rainfall increase is one possibility. Some estimates suggest that mean annual rainfall needed was more than 1200 mm (Quade et al., 2018). Egyptian mid Pleistocene basin-specific studies point to lower values of 400–900 mm/yr to maintain stable lake levels (Kieniewicz and Smith, 2009), and 200–600 mm/yr derived from the faunas drawn in SW Egyptian rock art (Haynes Jr. and Mead, 1987). Simplistically, if the current northern Libyan, Atlantic-influenced climate (annual precipitation 250–500 mm/yr; Saaed et al., 2019) shifted southward during humid intervals, more rainfall events concentrated in autumn–winter would be expected to enhance mean annual precipitation (Fig. 7 of Armon et al., 2024). This could be seen as an expansion of the spatial extent of the January mean $\delta^{18}\text{O}$ (-7.4% to -5.5% ; Fig. 16d) which is currently focussed in NW Libya, along with some additional lower values to $\sim -8\%$ to -6% .

The most compelling modern analogues for lake-filling precipitation sources north of the central Sahara watershed are the infrequent extreme rainfall events, which produce ephemeral desert lakes (Copernicus, 2023; NASA, 2024). These extreme events are also the most likely contributors to the modern groundwater-fed lakes of the Awbari Sand Sea (Burdon and Gonfiantini, 1991; Parker et al., 2008). The detailed evaluation of Rieder et al. (2025) for the modern Sebkha el Melah in Morocco suggests that the most significant (autumn focussed) lake filling events are not related to changes in mean annual precipitation, but instead to changes in rainfall intensity, frequency and several ingredients in the synoptic patterns of rainfall delivery. These extreme precipitation events in North Africa may be in-part linked to conditions derived from those generating atmospheric rivers, also called Atlantic tropical plumes (Akbari et al., 2019; Couper et al., 2025), which are projected to increase in a warmer world (Massoud et al., 2020). Lower $\delta^{18}\text{O}$ generated with extreme precipitation intensity (Yapp, 1982) tallies well with groundwater recharge events which are expected to be similarly biased to larger events. A secondary possibility is the expansion of summertime monsoon rainfall of high intensity (often associated with diurnal convection), which could be caused by eastward transfer of the modern situation in the western Sahara (and Algeria), which is more influenced by summertime extreme events (Armon et al., 2024).

7.4.5. Numerical climate models

The most convincing evidence for monsoonal rainfall is from sapropel-bearing units in the eastern Mediterranean, where there is a strong precession-related relationship with River Nile discharge, principally sourced from the Ethiopian Highlands, which were within the influence of the East African Monsoon at present and in the past (Revel et al., 2010; Rohling et al., 2015). This Mediterranean -focussed linkage has been supported by some palaeoclimate models which suggest monsoonal rainfall penetrating north of the central Saharan watershed at $\sim 21^\circ\text{N}$ (Pomposi et al., 2015; Tierney et al., 2017), including into the Fezzan (Reade et al., 2016), a situation which is likely to be more regionally variable (Cheddadi et al., 2021; Couper et al., 2025). However, if modern analogues suggest extreme rainfall events are key to lake filling events, then it is not clear that using mean annual precipitation from numerical models aids in predicting the water sources of Fezzan lakes. Also, in the western Mediterranean during the Quaternary and Late Miocene moisture availability was related to Atlantic-derived cyclones (Marzocchi et al., 2019), or more nuanced moisture sources involving Atlantic tropical plumes (Couper et al., 2025; Akbari et al., 2019). Here sediment cyclicity was still precession-forced, a pacing which by itself is not indicative of rainfall from the summer monsoon (Kutzbach et al., 2014).

In summary, beyond numerical climate models there is scant evidence for northward transfer of the summer monsoons as an important contributor to lakes in the Fezzan. The western Sahara was likely impacted rather differently (Couper et al., 2025). Instead, fossil groundwater isotopic data, and the probable delivery of lake and groundwater recharge through enhancement frequency and intensity of extreme events sourced from largely westerly-derived moisture holds

the key to lake generation in the Fezzan. This case for the Fezzan is by no means certain and requires biologic-sourced indicators of rainfall season to resolve the balance between southerly tropical/monsoonal and westerly sourced rainfall. An additional caveat is that these conclusions are better constrained for the mid Holocene and Late Quaternary, than the Pliocene and late Miocene succession of the Zarzur Fm, although the similarity in less evolved $\delta^{18}\text{O}$ ranges implies similarity in water sources.

7.5. Implications for the green Sahara hypothesis

The hypothesis of Larrasoña et al. (2013) is that green Sahara intervals (as expressed in Mediterranean sapropels; Fig. 17A) were promoted strongly by eccentricity modulation of the insolation signal largely related to precession. Whilst there is some synchronicity of the C2 and C3 carbonates with eccentricity modulation peaks at ca. 4.6 and ca. 5 Ma (Fig. 17C), data from the Zarzur Fm suggest the longer-scale pacing of wetter intervals in the Fezzan is more similar to the record of deep lakes from the East Africa rift which have a ca. 0.5 Myr pacing before 3 Ma (Trauth et al., 2007; Maslin et al., 2014; light blue bars in Fig. 17A,C). This pacing does not necessarily implicate monsoonal sourced rainfall in North Africa (Kutzbach et al., 2014). The C3 carbonate has a close match in timing with lake basins in the central Kenya Rift (Trauth et al., 2007), and the C2 carbonate is ca. 0.5 Myr older, coinciding with an eccentricity maximum (Fig. 17C). It is possible that the undated C4 carbonate may correspond to the east African deep lakes developed at ca. 4 Ma in the Turkana and Afar basins (Trauth et al., 2007). The C1 carbonate is less securely dated but is likely coeval with chron C3An.2n at ca. 6.4–6.8 Ma (Figs. 4, 13), falling in an interval in the East African Rift basins with only fluvial records. Given the synchronicity between east African and Saharan humid periods from 4.6 Ma, and the presence of hominins in eastern Africa at this time (Fig. 17;

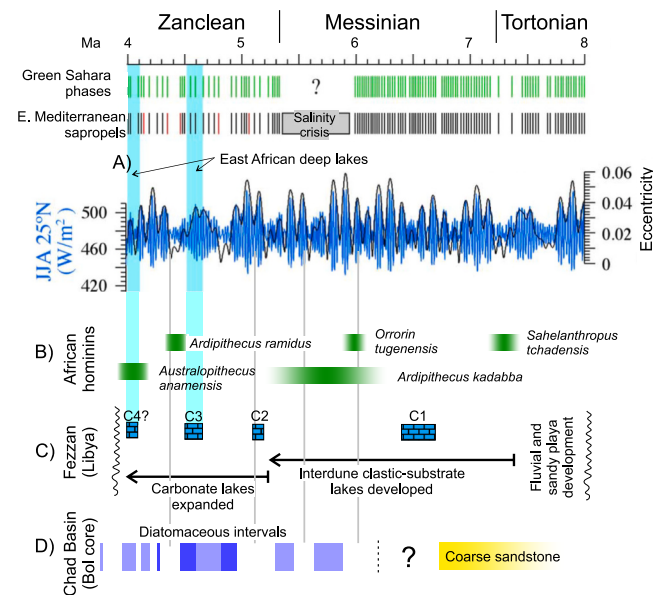


Fig. 17. Summary of environmental conditions in the Fezzan (in C), placed against the hypothesised green-Sahara episodes of Larrasoña et al. (2013), based on the eastern Mediterranean sapropel record, and summer eccentricity forcing of insolation (JJA) at 25°N (in A). C1 to C4 are carbonates in the Bir az Zallaf Mb, compared to east African deep lake development (Maslin et al., 2014, light blue bars). B) Age ranges of early hominins from Su (2024). Sahelanthropus tchadensis is from the northern Chad Basin. D) Diatomaceous intervals (dark blue = diatomites) in the lower part of the Bol core from the Chad Basin (from Novello et al., 2015, using the age model in their Fig. 5). Grey lines connect the middle of major argillaceous intervals to the eccentricity scale in A. (For interpretation of the references to colour in this figure legend, the reader is referred to the web version of this article.)

White et al., 2009; Leakey et al., 1998), it is possible that their range also included the Sahara.

The Zarzur Fm is comparable in age to the older part of the succession representing Megalake Chad (Novello et al., 2015; Moussa et al., 2021), which appears to extend to at least ~8 Ma (Lebatard et al., 2008; Novello et al., 2017). There, the central part of the lake system as expressed in the Bol core has alternations of argillaceous and diatomaceous lithologies (Fig. 17D). Modern river discharge into Lake Chad suggests that the more argillaceous intervals reflect larger freshwater inputs, and the diatom-rich parts reflect lower river discharge (and dryer intervals), with less argillaceous input (Moussa et al., 2016). There is not a clear correspondence between these Chad Basin wetter intervals and the C1-C4 limestones in the Fezzan, or between the Chad Basin intervals and the bundled peaks in insolation cycles driven by eccentricity (Fig. 17A, D). This indicates that lake filling-episodes of Megalake Chad and those in the Fezzan were decoupled. Perhaps significantly, both Saharan basins contain no clear expression of change timed to the Mediterranean salinity crisis. Further work needs to be done to understand the hydrological-sediment characteristics of these lake systems, which were some ~1400 km apart, separated by the Tibesti Mountains. These mountains likely offered a more equitable climate during humid intervals and a likely refugium for taxa during dryer intervals (Dinies et al., 2021).

The age of the Zarzur Fm overlaps the occurrence of the earliest hominins (Fig. 17B), with *Sahelanthropus tchadensis* from the Djurab Desert of northern Chad (Brunet et al., 2002; Lebatard et al., 2008) being the most proximal to the Fezzan. Other hominin species are found in eastern Africa during the interval of Zarzur Fm deposition, with clear connections between humid periods in both regions. These early hominins occupied more varied, wet and wooded habitats than later hominins which preferred grasslands (Su, 2024). In the northern Megalake Chad Basin, the earlier environment (~8–5 Ma) may have been more similar to that expressed in the Zarzur Fm with aeolian dunes and palmgrove woodland marginal to lakes, with associated river and marsh environments. Grasslands dominated after 4.5 Ma (Novello et al., 2017) with the woodland to grassland transition occurring between 7 Ma and 4.5 Ma, which was coeval with the lake systems developed in the Zarzur Fm. Whilst no vertebrate fossils are currently known from the Zarzur Fm and the biome conditions in the Fezzan in this interval are less understood than in eastern Africa and northern Chad, this work enhances the possibility of connections to these regions and that a ~1400 km transit across the Tibesti Mountains, with its refugia allowing early hominins to occupy habitats in the Fezzan like those in northern Chad.

8. Conclusions

Magnetostratigraphy from four sections indicates a composite polarity pattern comprising ten magnetozones, and two tentative normal polarity submagnetozones. This is statistically best matched with an interval from the latest Tortonian (late Miocene; magnetochron C3Br.3r) through to the middle Zanclean (magnetochron C3n.1r). A short section from the basal Zarzur Fm probably extends into C4n.2n of the late Tortonian and indicates an age range of ~8–4.3 Ma for this formation.

Sedimentological assessment of the Zarzur Fm from southern Libya indicates that this unit comprises several facies, with a range from minor amounts of pristine aeolian sandstone to more substantial amounts of sandstone with rhizoliths, probably representing a range of environments from vegetated aeolian dunes to vegetated siliciclastic lake margin deposits, much like those in comparable age successions associated with Megalake Chad. The lower part of the Zarzur Fm likely had a strong fluvial input, as evidenced by pebbly sandstones and fluvially-transported sand-sized mud aggregates. Sandy playa systems may have been important components in the lower part of the formation. This evolved into a lacustrine-aeolian dune depositional system in the

upper parts of the formation. Lacustrine facies are of two types; laminated dolomitic-wackstone-mudstones and gastropod and ostracod bearing calcareous sandstones formed on siliciclastic substrate lakes. The carbonates largely formed in saline lake systems, which were sometimes more evaporitic, and less frequently low salinity lakes. Lateral variability of nearby sections and facies attest to lake system formation in inter-dune depressions, as supported by the present-day outcrop pattern of lacustrine carbonates. A modern analogue for the range of environments present is the modern Ounianga Lakes of northern Chad. Stable isotopes of carbon and oxygen suggest that the lake systems varied in salinity, with dominantly low salinity, and a probable strong contribution from groundwater recharge, a water discharge mechanism that is compatible with the inter-dune lake systems inferred. The rainfall source for the lakes was dominantly from westerly derived cyclonic systems as infrequent extreme events, and probably less so from southerly derived summer monsoon rainfall. Magnetostratigraphic dating demonstrates a comparable pacing for the peaks in lacustrine development in the Fezzan, to the deep lake systems developed in the east African Rift during the Early Pliocene potentially allowing expansion of hominin ranges from eastern Africa into the Sahara region. The presence of early hominins in northern Chad at a time when the Fezzan was humid and the proximity between the two regions also suggests that early hominins could have used this route for dispersal north of the Central Saharan watershed.

Credit authorship contribution statement

Mark W. Hounslow: Writing – original draft, Visualization, Validation, Supervision, Software, Resources, Project administration, Methodology, Investigation, Formal analysis, Data curation, Conceptualization. **Helena E. White:** Writing – original draft, Visualization, Validation, Resources, Methodology, Investigation, Formal analysis, Conceptualization. **Nick Drake:** Writing – original draft, Visualization, Validation, Supervision, Resources, Project administration, Methodology, Investigation, Funding acquisition, Formal analysis, Conceptualization. **Vassil Karloukovski:** Writing – original draft, Visualization, Validation, Methodology, Investigation, Formal analysis. **Sue J. McLaren:** Writing – original draft, Validation, Supervision, Project administration, Methodology, Funding acquisition, Conceptualization. **Mustafa J. Salem:** Writing – original draft, Validation, Resources, Project administration, Investigation, Funding acquisition, Conceptualization. **Ahmed S. El-Hawat:** Writing – original draft, Visualization, Validation, Resources, Investigation, Formal analysis. **Osama Hlal:** Writing – original draft, Validation, Investigation.

Declaration of competing interest

The authors declare that they have no known competing financial interests or personal relationships that could have appeared to influence the work reported in this paper.

Acknowledgments

Fieldwork logistics would not have been possible without Toby Savage and Kevin White. Fieldwork support was from Repsol/REMSA and David Mattingly's field teams (supported from the Society for Libyan Studies Desert Migrations Project) along with logistic and financial support provided by the University of Benghazi Research Centre. ASH acknowledges the assistance of Dr. Awad Bilal. The Libyan Dept of Antiquities assisted with desert permits. Some palaeomagnetic data were measured by Matt Riding, but most were obtained by HEW during a self-funded PhD. Ulrich Salzmann attempted the pollen analysis. The reviewers Andy Roberts and anonymous offered many useful suggestions for improvement.

Appendix A. Supplementary data

Supplementary data to this article can be found online at <https://doi.org/10.1016/j.palaeo.2025.113187>.

Data availability

The data from this work, and the age model assessments are available on figshare (Hounslow and White, 2024), with additional data in the Supplementary Information.

References

- Abdullah, M., 2010. Petrography and Facies of the Al-Mahruqah Formation in the Murzuq Basin, SW Libya (PhD thesis). Universität Hamburg, p. 101.
- Abotalib, A.Z., Sultan, M., Elkadiri, R., 2016. Groundwater processes in Saharan Africa: Implications for landscape evolution in arid environments. *Earth Sci. Rev.* 156, 108–136.
- Abouelmagd, A., Sultan, M., Milewski, A., Kehew, A.E., Sturchio, N.C., Soliman, F., Krishnamurthy, R.V., Cutrim, E., 2012. Toward a better understanding of palaeoclimatic regimes that recharged the fossil aquifers in North Africa: Inferences from stable isotope and remote sensing data. *Palaeogeogr. Palaeoclimatol. Palaeoecol.* 329, 137–149.
- Abu-Zied, R.H., Keatings, K., Flower, R.J., Leng, M.J., 2011. Benthic foraminifera and their stable isotope composition in sediment cores from Lake Qarun, Egypt: changes in water salinity during the past~ 500 years. *J. Paleolimnol.* 45, 167–182.
- Akbary, M., Salimi, S., Hosseini, S.A., Hosseini, M., 2019. Spatio-temporal changes of atmospheric rivers in the Middle East and North Africa region. *Int. J. Climatol.* 39, 3976–3986.
- Amarathunga, U., Rohling, E.J., Grant, K.M., Francke, A., Latimer, J., Klaebe, R.M., Heslop, D., Roberts, A.P., Hutchinson, D.K., 2024. Mid-Pliocene glaciation preceded by a 0.5-million-year North African humid period. *Nat. Geosci.* 17, 660–666.
- Anderson, N.J., Leng, M.J., 2004. Increased aridity during the early Holocene in West Greenland inferred from stable isotopes in laminated-lake sediments. *Quat. Sci. Rev.* 23, 841–849.
- Andrews, J.N., 1993. Isotopic composition of groundwater and palaeoclimate at aquifer recharge. In: International Atomic Energy Agency (Ed.), *Isotope Techniques in the Study of Past and Current Environmental Changes in the Hydrosphere and the Atmosphere. Proceedings of a Symposium*, 19–23 April, 1993. IAEA, Vienna, pp. 271–292.
- Armitage, S.J., Drake, N.A., Stokes, S., El-Hawat, A.S., Salem, M.J., White, K., Turner, P., McLaren, S.J., 2007. Multiple phases of North African humidity recorded in lacustrine sediments from the Fezzan Basin, Libyan Sahara. *Quat. Geochronol.* 2, 181–186.
- Armon, M., de Vries, A.J., Marra, F., Peleg, N., Wernli, H., 2024. Saharan rainfall climatology and its relationship with surface cyclones. *Weath. Clim. Extremes* 43, <https://doi.org/10.1016/j.wace.2023.100638>.
- Baioumy, H., Kayanne, H., Tada, R., 2011. Record of Holocene aridification (6000–7000 BP) in Egypt (NE Africa): authigenic carbonate minerals from laminated sediments in Lake Qarun. *Quat. Int.* 245, 170–177.
- Bar-Matthews, M., Ayalon, A., Gilmour, M., Matthews, A., Hawkesworth, C.J., 2003. Sea-land oxygen isotopic relationships from planktonic foraminifera and speleothems in the Eastern Mediterranean region and their implication for paleorainfall during interglacial intervals. *Geochim. Cosmochim. Acta* 67, 3181–3199.
- Beyerle, U., Rueedi, J., Leuenberger, M., Aeschbach-Hertig, W., Peeters, F., Kipfer, R., Dodo, A., 2003. Evidence for periods of wetter and cooler climate in the Sahel between 6 and 40 kyr BP derived from groundwater. *Geophys. Res. Lett.* 30, <https://doi.org/10.1029/2002GL016310>.
- Borówka, R.K., Strobel, W., Halas, S., 2012. Stable isotope composition of subfossil *Cerastoderma glaucum* shells from the Szczecin Bay brackish deposits and its palaeogeographical implications (South Baltic Coast, Poland). *Quat. Res.* 77, 245–250.
- Bouchez, C., Goncalves, J., Deschamps, P., Vallet-Coulomb, C., Hamelin, B., Doumang, J.C., Sylvestre, F., 2016. Hydrological, chemical, and isotopic budgets of Lake Chad: a quantitative assessment of evaporation, transpiration and infiltration fluxes. *Hydrol. Earth Syst. Sci.* 20, 1599–1619.
- Bowen, G.J., Wassenaar, I.I., Hobson, K.A., 2005. Global application of stable hydrogen and oxygen isotopes to wildlife forensics. *Oecologia* 143, 337–348.
- Breecker, D.O., Sharp, Z.D., McFadden, L.D., 2009. Seasonal bias in the formation and stable isotopic composition of pedogenic carbonate in modern soils from Central New Mexico, USA. *Geol. Soc. Am. Bull.* 121, 630–640.
- Bruden, J.C., Arthur, G.R., 1981. Precision of measurement of remanent magnetization. *Can. J. Earth Sci.* 18, 527–538.
- Brunet, M., Guy, F., Pilbeam, D., Mackaye, H.T., Likius, A., Ahounta, D., Beauvilain, A., Blondel, C., Bocherens, H., Boissière, J.R., De Bonis, L., 2002. A new hominid from the Upper Miocene of Chad, Central Africa. *Nature* 418, 145–151.
- Burdon, D.J., Gonfiantini, R., 1991. Lakes in the Awbari sand sea of Fezzan, Libya. In: Salem, M.J., Belaid, M.N. (Eds.), *The Geology of Libya*, vol. 5. Elsevier, Amsterdam, pp. 2027–2041.
- Cancellieri, E., 2021. A tentative tale of Stone Age human dynamics in Pleistocene southwestern Libya (central Sahara). *Libyan Stud.* 52, 36–53.
- Causse, C., Hillaire-Marcel, C., 1988. Radiochronologies fondees sur le desequilibre (par defaut/par excess) du ^{230}Th appliques a l'étude de lacs Africains: Wadi Shati (Libye) et Natron, Magadi (Kenya-Tanzanie). In: Faure, H., Faure-Denard, L., Diop, E.S. (Eds.), *Changements Globaux en Afrique durant le Quaternaire—Passé, Présent, Future. INQUA-ASEQUA Symposium*, Dakar, 21–28th April, 1986. Centre National De La Recherche Scientifique, Paris, pp. 61–66.
- Cerling, T.E., 1992. Development of grasslands and savannas in East Africa during the Neogene. *Glob. Planet. Chang.* 5, 241–247.
- Cerling, T.E., Wynn, J.G., Andanje, S.A., Bird, M.I., Korir, D.K., Levin, N.E., Mace, W., Macharia, A.N., Quade, J., Remien, C.H., 2011. Woody cover and hominin environments in the past 6 million years. *Nature* 476, 51–56.
- Cheddadi, R., Carré, M., Nourelbait, M., François, L., Rhoujjati, A., Manay, R., Ochoa, D., Scheufb, E., 2021. Early Holocene greening of the Sahara requires Mediterranean winter rainfall. *Proc. Natl. Acad. Sci.* 118, e2024898118. <https://doi.org/10.1073/pnas.2024898118>.
- Copernicus, 2023. Storm Daniel Causes Flooding in Libya. <https://www.copernicus.eu/en/media/image-day-gallery/storm-daniel-causes-flooding-libya>.
- Couper, H.O., Day, C.C., Barrott, J.J., Hollowood, S.J., Carolin, S.A., Lovett, B., Bouzouggar, A., Barton, N., Henderson, G.M., 2025. Evidence for the role of tropical plumes in driving mid-Holocene north-west Sahara rainfall. *Earth Planet. Sci. Lett.* 652, 119195. <https://doi.org/10.1016/j.epsl.2024.119195>.
- Creutz, M., Van Bocxlaer, B., Abderamane, M., Verschuren, D., 2016. Recent environmental history of the desert oasis lakes at Ounianga Serir, Chad. *J. Paleolimnol.* 55, 167–183.
- Crocker, J.A., Naafs, B.D.A., Westerhold, T., James, R.H., Cooper, M.J., Röhli, U., Pancost, R.D., Xuan, C., Osborne, C.P., Beerling, D.J., Wilson, P.A., 2022. Astronomically controlled aridity in the Sahara since at least 11 million years ago. *Nat. Geosci.* 15, 671–676.
- Cromwell, G., Johnson, C.L., Tauxe, L., Constable, C.G., Jarboe, N.A., 2018. PSV10: a global data set for 0–10 Ma time-averaged field and paleosecular variation studies. *Geochem. Geophys. Geosyst.* 19, 1533–1558.
- Deenen, M.H., Langereis, C.G., van Hinsbergen, D.J., Biggin, A.J., 2014. Erratum: geomagnetic secular variation and the statistics of palaeomagnetic directions. *Geophys. J. Int.* 197, 643.
- Desio, A., 1971. Outline and problems of the Geomorphological evolution of Libya from the Tertiary to the present day. In: Gray, C. (Ed.), *Symposium on the Geology of Libya, Tripoli April 14–18th, 1969*. Faculty of Science, Univ. of Libya, Tripoli, pp. 11–36.
- Dinies, M., Schimmel, L., Hoelzmann, P., Kröpelin, S., Darius, F., Neef, R., 2021. Holocene high-altitude vegetation dynamics on Emi Koussi, Tibesti mountains (Chad, central Sahara). In: Runge, J., Gosling, W.D., Lézine, A.-M., Scott, L. (Eds.), *Quaternary Vegetation Dynamics—The African Pollen Database*. Taylor and Francis, pp. 27–50. <https://doi.org/10.1201/9781003162766-4>.
- Dodo, A., Zuppi, G.M., 1997. Étude des écoulements souterrains dans le bassin de Bilma-Djado à l'aide des isotopes de l'environnement. *Compt. Rend. l'Acad. Sci. Ser. II Earth Planet. Sci.* 325, 845–852.
- Drake, N., Breeze, P., 2016. Climate change and modern human occupation of the Sahara from MIS 6–2. In: Jones, S.C., Stewart, B.A. (Eds.), *Africa from MIS 6–2, Population Dynamics and Paleoenvironments*. Springer, pp. 103–122.
- Drake, N.A., El-Hawat, A.S., Turner, P., Armitage, S.J., Salem, M.J., White, K.H., McLaren, S.J., 2008. Palaeohydrology of the Fezzan Basin and surrounding regions: the last 7 million years. *Palaeogeogr. Palaeoclimatol. Palaeoecol.* 263, 131–145.
- Drake, N.A., Blench, R.M., Armitage, S.J., Bristow, C.S., White, K.H., 2011. Ancient watercourses and biogeography of the Sahara explain the peopling of the desert. *Proc. Natl. Acad. Sci. USA* 108, 458–462.
- Drake, N.A., Lem, R.E., Armitage, S.J., Breeze, P., Francke, J., El-Hawat, A.S., Salem, M.J., Hounslow, M.W., White, K., 2018. Reconstructing palaeoclimate and hydrological fluctuations in the Fezzan Basin (southern Libya) since 130 ka: a catchment-based approach. *Quat. Sci. Rev.* 200, 376–394.
- Drake, N.A., Candy, I., Breeze, P., Armitage, S.J., Gasmi, N., Schwenninger, J.L., Peat, D., Manning, K., 2022. Sedimentary and geomorphic evidence of Saharan megakalages: a synthesis. *Quat. Sci. Rev.* 276. <https://doi.org/10.1016/j.quascirev.2021.107318>.
- Edmunds, W.M., Dodo, A., Djoret, D., Gaye, C.H., Goni, I.B., Travi, Y., Zouari, K., Zuppi, G.M., Gasse, F., 2004. Groundwater as an archive of climatic and environmental change: Europe to Africa. In: Battarbee, R.W., Stickley, C.E. (Eds.), *Past Climate Variability through Europe and Africa*. Springer, Dordrecht, pp. 279–306.
- El-Hawat, A.S., El-Ghali, M.A.K., McLaren, S.J., Kemp, S.J., 2021. Early silicification of the Cyrenaican chert, Libya: the importance of moganite as a transitional silicon dioxide phase. *Sedimentology* 68, 855–880.
- El-Shenawy, M.I., Kim, S.T., Schwarzc, H.P., Asmerom, Y., Polyak, V.J., 2018. Speleothem evidence for the greening of the Sahara and its implications for the early human dispersals out of sub-Saharan Africa. *Quat. Sci. Rev.* 188, 67–76.
- Farrell, K.M., Harris, W.B., Mallinson, D.J., Culver, S.J., Riggs, S.R., Pierson, J., Self-Tailor, J.M., Lautier, J.C., 2012. Standardizing texture and facies codes for a process-based classification of clastic sediment and rock. *J. Sediment. Res.* 82, 364–378.
- Foley, R.A., Mafllo-Fernández, J.M., Mirazón Lahr, M., 2013. The Middle Stone Age of the Central Sahara: Biogeographical opportunities and technological strategies in later human evolution. *Quat. Int.* 300, 153–170.
- Fontes, J.-C., Gasse, F., Andrews, J.N., 1993. Climatic conditions of Holocene groundwater recharge in the Sahel zone. In: International Atomic Energy Agency (Ed.), *Isotope Techniques in the Study of Past and Current Environmental Changes in the Hydrosphere and the Atmosphere. Proceedings of a Symposium*, 19–23 April, 1993. IAEA, Vienna, pp. 231–248.
- Gasse, F., 2000. Hydrological changes in the African tropics since the last Glacial Maximum. *Quat. Sci. Rev.* 19, 189–211.

- Gasse, F., Fontes, J.C., Plaziat, J.C., Carbonel, P., Kaczmarska, I., De Deckker, P., Soulié-Marsche, I., Callot, Y., Dupeuble, P.A., 1987. Biological remains, geochemistry and stable isotopes for the reconstruction of environmental and hydrological changes in the Holocene lakes from North Sahara. *Palaeogeogr. Palaeoclimatol. Palaeoecol.* 60, 1–46.
- Gaven, C., Hillaire-Marcel, C., Petit-Maire, N., 1981. A Pleistocene lacustrine episode in southeastern Libya. *Nature* 290, 131–133.
- Geyh, M.A., Thiedig, F., 2008. The Middle Pleistocene Al Mahrugah Formation in the Murzuq Basin, northern Sahara, Libya evidence for orbitally-forced humid episodes during the last 500,000 years. *Palaeogeogr. Palaeoclimatol. Palaeoecol.* 257, 1–21.
- Gierz, P., Werner, M., Lohmann, G., 2017. Simulating climate and stable water isotopes during the last interglacial using a coupled climate-isotope model. *J. Adv. Model. Earth Syst.* 9, 2027–2045. <https://doi.org/10.1002/2017MS001056>.
- Givon, Y., Hess, O., Flaounas, E., Catto, J.L., Sprenger, M., Raveh-Rubin, S., 2024. Process-based classification of Mediterranean cyclones using potential vorticity. *Weaht. Clim. Dyn.* 5, 133–162.
- Goni, I.B., Fellman, E., Edmunds, W.M., 2001. Rainfall geochemistry in the Sahel region of northern Nigeria. *Atmos. Environ.* 35, 4331–4339.
- Griffin, D.L., 1999. The late Miocene climate of northeastern Africa: unravelling the signals in the sedimentary succession. *J. Geol. Soc. Lond.* 156, 817–826.
- Grine, F.E., 2016. The late Quaternary hominins of Africa: The skeletal evidence from MIS 6–2. In: Jones, S.C., Stwart, B.A. (Eds.), *Africa from MIS 6–2, Population Dynamics and Paleoenvirons*. Springer, pp. 323–381.
- Haynes Jr., C.V., 2001. Geochronology and climate change of the Pleistocene–Holocene transition in the Darb el Arba'in Desert, Eastern Sahara. *Geoarchaeology* 16, 119–141.
- Haynes Jr., C.V., Mead, A.R., 1987. Radiocarbon dating and paleoclimatic significance of subfossil *Limicolaria* in northwestern Sudan. *Quat. Res.* 28, 86–99.
- Herold, M., Lohmann, G., 2009. Eemian tropical and subtropical African moisture transport: an isotope modelling study. *Clim. Dyn.* 33, 1075–1088.
- Hillaire-Marcel, C., 1982. Paléohydrologie isotopique. In: Petit-Maire, N. (Ed.), *Le Shati: Lac Pléistocène du Fezzan (Libye)*. CNRS, Paris, pp. 34–43.
- Horton, T.W., Defliese, W.F., Tripathi, A.K., Oze, C., 2016. Evaporation induced 18O and 13C enrichment in lake systems: a global perspective on hydrologic balance effects. *Quat. Sci. Rev.* 131, 365–379.
- Hounslow, M.W., 2023a. Palaeomag-Tools, Version 5.1a. Figshare. Software. <https://doi.org/10.6084/m9.figshare.24167190.v1>.
- Hounslow, M.W., 2023b. A DOSBox Version of LINEFIN of Kent, Briden and Mardia (1983). figshare. Software. <https://doi.org/10.6084/m9.figshare.24826617.v1>.
- Hounslow, M.W., White, H.E., 2024. The magnetostratigraphic and stable carbon and oxygen isotopic dataset for the Zarzur Formation in Wadi ash Shati, Libya. Figshare Dataset. <https://doi.org/10.6084/m9.figshare.26771125>.
- Hounslow, M.W., Posen, P.E., Warrington, G., 2004. Magnetostratigraphy and biostratigraphy of the upper Triassic and lowermost Jurassic succession, St. Audrie's Bay, UK. *Palaeogeogr. Palaeoclimatol. Palaeoecol.* 213, 331–358.
- Hounslow, M.W., White, H.E., Drake, N.A., Salem, M.J., El-Hawat, A.S., McLaren, S.J., Karloukovski, V., Noble, S.R., Hlal, O., 2017. Miocene humid intervals and establishment of drainage networks by 23 Ma in the Central Sahara, southern Libya. *Gondwana Res.* 45, 118–137.
- Hounslow, M.W., Harris, S.E., Wójcik, K., Nawrocki, J., Ratcliffe, K.T., Woodcock, N.H., Montgomery, P., 2021. A geomagnetic polarity stratigraphy for the Middle and Upper Ordovician. *Palaeogeogr. Palaeoclimatol. Palaeoecol.* 567, 110225. <https://doi.org/10.1016/j.palaeo.2021.110225>.
- Hounslow, M.W., Xuan, C., Nilsson, A., 2022. Chapter 5: Using the geomagnetic field for correlation and dating. In: Coe, A.L. (Ed.), *Deciphering Earth's History: The Practice of Stratigraphy*. Geological Society of London, Bath, pp. 81–99.
- Icole, M., Riser, J., 1982. Les Formations Paleolacustres: Cadre Géologique et Morphologie. In: Petit-Maire, N. (Ed.), *Le Shati: Lac Pleistocene du Fezzan (Libye)*. Editions du CNRS, Paris, pp. 11–27.
- Indahl, U.G., Næs, T., Liland, K.H., 2018. A similarity index for comparing coupled matrices. *J. Chemom.* 32. <https://doi.org/10.1002/cem.3049>.
- IRC, 1985. 1:1,000,000 Geological Map of Libya. Industrial Research Centre, Tripoli.
- James, N.P., Bone, Y., 2022. Sedimentology and diagenesis of Pleistocene calcareous, non-dolomitic, interdune sediments, Coorong Coastal Plain, South Australia. *Sedimentology* 69, 2814–2843.
- Jasechko, S., 2016. Late-Pleistocene precipitation ^{18}O interpolated across the global landmass. *Geochim. Geophys. Geosyst.* 17, 3274–3288.
- Jiang, Y., Li, J., Zuo, R., Sun, C., Zhai, Y., Tian, L., Dai, W., Wang, S., Shang, Z., Liu, Y., Jiao, X., 2024. The transmission of isotopic signals from precipitation to groundwater and its controls: an experimental study with soil cylinders of various soil textures and burial depths in a monsoon region. *J. Hydrol.* 631. <https://doi.org/10.1016/j.jhydrol.2024.130746>.
- Joseph, A., Aranyossy, J.F., Kanta, I., 1990. Recharges et paléo-recharges des aquifères discontinus du socle de l'Air (Niger). *Geodin. Acta* 4, 185–197.
- Joseph, A., Frangi, J.P., Aranyossy, J.F., 1992. Isotope characteristics of meteoric water and groundwater in the Sahelo-Sudanese zone. *J. Geophys. Res. Atmos.* 97, 7543–7551.
- Josse, J., Holmes, S., 2016. Measuring multivariate association and beyond. *Stat. Surv.* 10, 132–167. <https://doi.org/10.1214/16-SS116>.
- Kent, J.T., Briden, J.C., Mardia, K.V., 1983. Linear and planar structure in ordered multivariate data as applied to progressive demagnetisation of palaeomagnetic remanence. *Geophys. J. R. Astron. Soc.* 81, 75–87.
- Kieniewicz, J.M., Smith, J.R., 2009. Paleoenvironmental reconstruction and water balance of a mid-Pleistocene pluvial lake, Dakhleh Oasis, Egypt. *Geol. Soc. Am. Bull.* 121, 1154–1171.
- Kindermann, K., Bubenzier, O., Nussbaum, S., Riemer, H., Darius, F., Pöllath, N., Mettan, U., 2006. Palaeoenvironment and holocene land use of Djara, western desert of Egypt. *Quat. Sci. Rev.* 25, 1619–1637.
- Koráb, T., 1984. Geological Map of Libya 1: 250 000. Sheet: Tmessa NG 33-7. Explanatory Booklet. Industrial Research Centre, Tripoli, p. 87.
- Kostadinova, M., Jordanova, N., Jordanova, D., Kovacheva, M., 2004. Preliminary study on the effect of water glass impregnation on the rock-magnetic properties of baked clay. *Stud. Geophys. Geod.* 48, 637–646.
- Kowalek, T., 2006. History of mollusc community types and faunal dynamics in continental saline ecosystems of the South Mediterranean Quaternary. *Riv. Ital. Paleontol. Stratigr.* 112, 275–286.
- Kutzbach, J.E., Chen, G., Cheng, H., Edwards, R.L., Liu, Z., 2014. Potential role of winter rainfall in explaining increased moisture in the Mediterranean and Middle East during periods of maximum orbitally-forced insolation seasonality. *Clim. Dyn.* 42, 1079–1095.
- Lallier, F., Antoine, C., Charreau, J., Caumon, G., Ruij, J., 2013. Management of ambiguities in magnetostratigraphic correlation. *Earth Planet. Sci. Lett.* 371, 26–36.
- Larrasoña, J.C., 2021. A review of West African monsoon penetration during Green Sahara periods: implications for human evolution and dispersals over the last three million years. *Oxford Open Clim. Change* 1. <https://doi.org/10.1093/oxclim/kgab011>.
- Larrasoña, J.C., Roberts, A.P., Rohling, E.J., 2013. Dynamics of green Sahara periods and their role in hominin evolution. *PLoS One* 8. <https://doi.org/10.1371/journal.pone.0076514>.
- Leakey, M.G., Feibel, C.S., MacDougall, I., Ward, C., Walker, A., 1998. New specimens and confirmation of an early age for *Australopithecus anamensis*. *Nature* 393, 62–66.
- Lebatard, A.E., Bourlès, D.L., Duringer, P., Jolivet, M., Braucher, R., Carcaillet, J., Schuster, M., Arnaud, N., Monié, P., Lihoreau, F., Likius, A., 2008. Cosmogenic nuclide dating of *Sahelanthropus tchadensis* and *Australopithecus bahrelghazali*: mio-Pliocene hominids from Chad. *Proc. Natl. Acad. Sci. USA* 105, 3226–3231.
- Leng, M.J., Marshall, J.D., 2004. Palaeoclimate interpretation of stable isotope data from lake sediment archives. *Quat. Sci. Rev.* 23, 811–831.
- Levin, N.E., 2015. Environment and climate of early human evolution. *Annu. Rev. Earth Planet. Sci.* 43, 405–429.
- Li, H.C., Ku, T.L., 1997. $\delta^{13}\text{C}$ – $\delta^{18}\text{C}$ covariance as a paleohydrological indicator for closed-basin lakes. *Palaeogeogr. Palaeoclimatol. Palaeoecol.* 133, 69–80.
- Maduabuchi, C., Faye, S., Maloszewski, P., 2006. Isotope evidence of palaeorecharge and palaeoclimate in the deep confined aquifers of the Chad Basin, NE Nigeria. *Sci. Total Environ.* 370, 467–479.
- Magee, J.W., Bowler, J.M., Miller, G.H., Williams, D.L.G., 1995. Stratigraphy, sedimentology, chronology and palaeohydrology of Quaternary lacustrine deposits at Madigan Gulf, Lake Eyre, South Australia. *Palaeogeogr. Palaeoclimatol. Palaeoecol.* 113, 3–42.
- Man, O., 2008. On the identification of magnetostratigraphic polarity zones. *Stud. Geophys. Geod.* 52, 173–186.
- Man, O., 2011. The maximum likelihood dating of magnetostratigraphic sections. *Geophys. J. Int.* 185, 133–143.
- Marzocchi, A., Flecker, R., Lunt, D.J., Krijgsman, W., Hilgen, F.J., 2019. Precessional drivers of late Miocene Mediterranean sedimentary sequences: African summer monsoon and Atlantic winter storm tracks. *Paleoceanogr. Paleoclimatol.* 34, 1980–1994. <https://doi.org/10.1029/2019PA003721>.
- Maslin, M.A., Brierley, C.M., Milner, A.M., Shultz, S., Trauth, M.H., Wilson, K.E., 2014. East African climate pulses and early human evolution. *Quat. Sci. Rev.* 101, 1–17.
- Massoud, E., Massoud, T., Guan, B., Sengupta, A., Espinoza, V., De Luna, M., Raymond, C., Waliser, D., 2020. Atmospheric rivers and precipitation in the Middle East and North Africa (MENA). *Water* 12, 2863. <https://doi.org/10.3390/w12102863>.
- Mattingley, D.J., Reynolds, T., Dore, J.N., 2003. Synthesis of Human Activities in Fazzān. In: Mattingley, D.J. (Ed.), *The Archaeology of Fazzān, 1 Synthesis*. Dept of Antiquities, Tripoli, pp. 327–373.
- McCrea, J.M., 1950. On the isotopic chemistry of carbonates and a paleotemperature scale. *J. Chem. Phys.* 18, 849–857.
- McFadden, P.L., McElhinny, M.W., 1988. The combined analysis of remagnetisation circles and direct observations in paleomagnetism. *Earth Planet. Sci. Lett.* 87, 161–172.
- McFadden, P.L., McElhinny, M.W., 1990. Classification of the reversal test in paleomagnetism. *Geophys. J. Int.* 103, 725–729.
- Merlo, S., Hakenbeck, S., Balbo, A.L., 2013. Desert migrations project XVIII: the archaeology of the northern Fazzān. A preliminary report. *Libyan Stud.* 44, 141–161.
- Mirazon Lahr, M., 2010. Saharan corridors and their role in the evolutionary geography of 'Out of Africa I'. In: Fleagle, J.G., Shea, J.J., Grine, F.E., Baden, A.L., Leakey, R.E. (Eds.), *Out of Africa I: The First Hominin Colonization of Eurasia*. Springer, pp. 27–46.
- Montgomery, P., Hailwood, E.A., Gale, A.S., Burnett, J.A., 1998. The magnetostratigraphy of Coniacian-late Campanian chalk sequences in southern England. *Earth Planet. Sci. Lett.* 156, 209–224.
- Mook, W.G., 1971. Paleotemperatures and chlorinities from stable carbon and oxygen isotopes in shell carbonate. *Palaeogeogr. Palaeoclimatol. Palaeoecol.* 9, 245–263.
- Moussa, A., Novello, A., Lebatard, A.E., Decarreau, A., Fontaine, C., Barboni, D., Sylvestre, F., Bourles, D.L., Paillès, C., Buchet, G., Duringer, P., 2016. Lake Chad sedimentation and environments during the late Miocene and Pliocene: New evidence from mineralogy and chemistry of the Bol core sediments. *J. Afr. Earth Sci.* 118, 192–204.
- Moussa, A., Mahamat Nour, A., Abderamane, H., Mackaye, H.T., Likius, A., Schuster, M., Duringer, P., Ghienne, J.-F., Vignaud, P., 2021. Analysis of the deposit

- conditions of sedimentary series of fluvio-lacustrine and aeolian origin in the Djourab desert, in Northern Chad. *Afr. J. Environ. Sci. Technol.* 15, 470–492.
- Muftah, A.M., Pavlakis, P., Godelitsas, A., Gamaletsos, P., Boaz, N., 2013. Paleogeography of the Eosahabi River in Libya: New insights into the mineralogy, geochemistry and paleontology of Member U1 of the Sahabi Formation, northeastern Libya. *J. Afr. Earth Sci.* 78, 86–96.
- Muller, R., Nyström, J.P., Wright, V.P., 2004. Pedogenic mud aggregates and paleosol development in ancient dryland river systems: criteria for interpreting alluvial mudrock origin and floodplain dynamics. *J. Sediment. Res.* 74, 537–551.
- NASA, 2024. A deluge for the Sahara. <https://earthobservatory.nasa.gov/images/153320/a-deluge-for-the-sahara>.
- Novello, A., Lebatard, A.E., Moussa, A., Barboni, D., Sylvestre, F., Bourlès, D.L., Paillès, C., Buchet, G., Decarreau, A., Düringer, P., Ghienne, J.F., 2015. Diatom, phytolith, and pollen records from a 10Be/9Be dated lacustrine succession in the Chad basin: Insight on the Miocene–Pliocene paleoenvironmental changes in Central Africa. *Palaeogeogr. Palaeoclimatol. Palaeoecol.* 430, 85–103.
- Novello, A., Barboni, D., Sylvestre, F., Lebatard, A.E., Paillès, C., Bourlès, D.L., Likius, A., Mackaye, H.T., Vignaud, P., Brunet, M., 2017. Phytoliths indicate significant arboreal cover at Sahelanthropus type locality TM266 in northern Chad and a decrease in later sites. *J. Hum. Evol.* 106, 66–83.
- Ogg, J.G., 2020. Geomagnetic polarity timescale. In: Gradstein, F.M., Ogg, J.G., Schmitz, M., Ogg, G. (Eds.), *The Geologic Time Scale 2020*, 1. Elsevier, pp. 159–192. <https://doi.org/10.1016/B978-0-12-824360-2.00005-X>.
- Olson, P., Hinov, L., Driscoll, P., 2014. Nonrandom geomagnetic reversal times and geodynamo evolution. *Earth Planet. Sci. Lett.* 38, 9–17.
- Pape, J.R., Banner, J.L., Mack, L.E., Musgrove, M., Guilfoyle, A., 2010. Controls on oxygen isotope variability in precipitation and cave drip waters, Central Texas, USA. *J. Hydrol.* 385, 203–215.
- Parizek, A., Klen, L., Röhlich, P., 1984. Geological Map of Libya 1:250,000, Sheet: Idri (NG 33-1), Explanatory Booklet. Industrial Research Centre, Tripoli.
- Parker, A., Harris, B., White, K., Drake, N., 2008. Phytoliths as indicators of grassland dynamics during the Holocene from lake sediments in the Ubari sand sea, Fazzan Basin, Libya. *Libyan Stud.* 39, 29–40.
- Perri, E., Tucker, M., 2007. Bacterial fossils and microbial dolomite in Triassic stromatolites. *Geology* 35, 207–210.
- Perri, E., Tucker, M.E., Slowakiewicz, M., Whitaker, F., Bowen, L., Perrotta, I.D., 2018. Carbonate and silicate biomineralisation in a hypersaline microbial mat (Mesaieed sabkha, Qatar): Roles of bacteria, extracellular polymeric substances and viruses. *Sedimentology* 65, 1213–1245.
- Petit-Maire, N. (Ed.), 1982. *Le Shati: Lac Pléistocène du Fezzan (Libye)*. CNRS, Paris.
- Petit-Maire, N., 1989. Interglacial environments in presently hyperarid Sahara: Palaeoclimatic implications. In: Leinen, M., Sarnthein, M. (Eds.), *Paleoclimatology and Paleometeorology: Modern and Past Patterns of Global Atmospheric Transport*. Kluwer Academic Publishers, pp. 637–661.
- Petit-Maire, N., 1991. Recent Quaternary climatic change and man in the Sahara. *J. Afr. Earth Sci.* 12, 125–132.
- Petit-Maire, N., 1994. Les variations climatiques au Sahara: du passé au fut. In: Alexandre, J., De Dapper, M., Symoens, J.-J. (Eds.), *Climatic Change and Geomorphology in Tropical Environment*, International Colloquium Brussels, 6 May 1992, pp. 149–166.
- Petit-Maire, N., Delibrias, G., Gaven, C., 1980. Pleistocene lakes in the Shati area, Fezzan (27°, 30°N). *Paleoecol. Afr.* 12, 289–295.
- Pomposi, C., Kushnir, Y., Giannini, A., 2015. Moisture budget analysis of SST-driven decadal Sahel precipitation variability in the twentieth century. *Clim. Dyn.* 44, 3303–3321. <https://doi.org/10.1007/s00382-014-2382-3>.
- Prendergast, A.L., Stevens, R.E., Barker, G., O'Connell, T.C., 2015. Oxygen isotope signatures from land snail (*Helix melanostoma*) shells and body fluid: Proxies for reconstructing Mediterranean and North African rainfall. *Chem. Geol.* 409, 87–98.
- Quade, J., Dente, E., Armon, M., Dor, Y.B., Morin, E., Adam, O., Enzel, Y., 2018. Megalakes in the Sahara? A review. *Quat. Res.* 90, 253–275.
- R Core Team, 2022. R: A Language and Environment for Statistical Computing. R Foundation for Statistical Computing, Vienna, Austria. <https://www.R-project.org/>.
- Reade, H., O'Connell, T.C., Barker, G., Stevens, R.E., 2016. Pleistocene and Holocene palaeoclimates in the Gebel Akhdar (Libya) estimated using herbivore tooth enamel oxygen isotope compositions. *Quat. Int.* 404, 150–162.
- Revel, M., Ducassou, E., Groussel, F.E., Bernasconi, S.M., Migeon, S., Révillon, S., Mascle, J., Murat, A., Zaragoza, S., Bosch, D., 2010. 100,000 years of African monsoon variability recorded in sediments of the Nile margin. *Quat. Sci. Rev.* 29, 1342–1362.
- Rieder, J.C., Aemisegger, F., Dente, E., Armon, M., 2025. Meteorological ingredients of heavy precipitation and subsequent lake-filling episodes in the northwestern Sahara. *Hydroclim. Earth Syst. Sci.* 29 (5), 1395–1427.
- Ritchie, J.C., Haynes, C.V., 1987. Holocene vegetation zonation in the eastern Sahara. *Nature* 330, 645–647.
- Rohling, E.J., Marino, G., Grant, K.M., 2015. Mediterranean climate and oceanography, and the periodic development of anoxic events (sapropels). *Earth Sci. Rev.* 143, 62–97.
- Rosso, J.C., Gaillard, J.M., 1982. Faunes d'invertébrés mollusques testacés (macrofaune). In: Petit-Maire, N. (Ed.), *Le Shati: Lac Pléistocène du Fezzan (Libye)*. CNRS, Paris, pp. 55–66.
- Rozanski, K., Araguás-Araguás, L., Gonfiantini, R., 1993. Isotopic patterns in modern global precipitation. In: Swart, P.K., Lohmann, K.C., McKenzie, J., Savin, S. (Eds.), Climate Change in Continental Isotopic Records, Geophysical Monograph, vol. 78, pp. 1–36.
- Rust, B.R., Nanson, G.C., 1989. Bedload transport of mud as pedogenic aggregates in modern and ancient rivers. *Sedimentology* 36, 291–306.
- Saaed, M.W., El-Barasi, Y.M., Rahil, R.O., 2019. Our present knowledge about the history and composition of the vegetation and flora of Libya. *Webbia* 74, 325–338.
- Salem, O., Visser, J.H., Dray, M., Gonfiantini, R., 1980. Groundwater Flow Patterns in the Western Libyan Arab Jamahiriya Evaluated from Isotopic Data. Arid-Zone Hydrology: Investigations with Isotope Techniques. IAEA, Vienna, Sti/Pub/547.
- Seidl, K., Röhlich, P., 1984. Geological Map of Libya, 1: 250 000. Sheet Sabha (NG 33-2). Explanatory Booklet, Industrial Research Centre, Tripoli, p. 93.
- Sheldon, N.D., Tabor, N.J., 2009. Quantitative paleoenvironmental and paleoclimatic reconstruction using paleosols. *Earth Sci. Rev.* 95, 1–52.
- Sonntag, C., Thorweiche, U., Rudolph, J., Loehnert, E.P., Junghans, C., Münnich, K.O., Klitzsch, E., El Shazly, E.M., Swailem, F., 1980. Paleoclimatic evidence in apparent ^{14}C ages of Saharan groundwaters. *Radiocarbon* 22, 871–878.
- Soulié-Märscle, I., 2008. Charophytes, indicators for low salinity phases in North African sebkhet. *J. Afr. Earth Sci.* 51, 69–76.
- Sturchio, N.C., Du, X., Purtshell, R., Lehmann, B.E., Sultan, M., Patterson, L.J., Lu, Z.T., Müller, P., Bigler, T., Bailey, K., O'Connor, T.P., 2004. One million year old groundwater in the Sahara revealed by krypton-81 and chlorine-36. *Geophys. Res. Lett.* 31, L05503. <https://doi.org/10.1029/2003GL019234>.
- Su, D.F., 2024. Early hominin paleoenvironments and habitat heterogeneity. *Annu. Rev. Anthropol.* 53, 21–35.
- Suganuma, Y., Okada, M., Head, M.J., Kameo, K., Haneda, Y., Hayashi, H., Irizuki, T., Itaki, T., Izumi, K., Kubota, Y., Nakazato, H., 2021. Formal ratification of the global boundary stratotype section and point (GSSP) for the Chibanian stage and middle Pleistocene subseries of the Quaternary system: the Chiba section, Japan. *Episodes J. Int. Geosci.* 44, 317–347.
- Sultan, M., Sturchio, N., Hassan, F.A., Hamdan, M.A.R., Mahmood, A.M., El Alfay, Z., Stein, T., 1997. Precipitation source inferred from stable isotopic composition of Pleistocene groundwater and carbonate deposits in the Western desert of Egypt. *Quat. Res.* 48, 29–37.
- Székely, G.J., Rizzo, M.L., 2017. The energy of data. *Annu. Rev. Stat. Appl.* 4, 447–479.
- Talbot, M.R., 1990. A review of the palaeohydrological interpretation of carbon and oxygen isotopic ratios in primary lacustrine carbonates. *Chem. Geol. Isotope Geosci. Sect.* 80, 261–279.
- Thiedig, F.M., Ozeen, D., El-Chair, M., Geyh, M.A., 2000. The absolute age of the Quaternary lacustrine limestone of the Al Mahrurah Formation — Murzuq Basin, Libya. In: Sola, M.A., Worsley, D. (Eds.), *Geological Exploration in the Murzuq Basin*. Elsevier, Amsterdam, pp. 89–116.
- Tierney, J.E., Pausata, F.S., deMenocal, P.B., 2017. Rainfall regimes of the Green Sahara. *Sci. Adv.* 3. <https://doi.org/10.1126/sciadv.1601503>.
- Tipple, B.J., Pagani, M., 2007. The early origins of terrestrial C4 photosynthesis. *Annu. Rev. Earth Planet. Sci.* 35, 435–461.
- Trauth, M.H., Maslin, M.A., Deino, A.L., Strecker, M.R., Bergner, A.G., Dühnforth, M., 2007. High-and low-latitude forcing of Plio-Pleistocene East African climate and human evolution. *J. Hum. Evol.* 53, 475–486.
- Tzedakis, P.C., 2007. Seven ambiguities in the Mediterranean palaeoenvironmental narrative. *Quat. Sci. Rev.* 26, 2042–2066.
- Van Boekelaer, B., Verschuren, D., Schettler, G., Kröpelin, S., 2011. Modern and early Holocene mollusc fauna of the Ounianga lakes (northern Chad): implications for the palaeohydrology of the Central Sahara. *J. Quat. Sci.* 26, 433–447.
- Warren, J.K., 1990. Sedimentology and mineralogy of dolomitic Coorong lakes, South Australia. *J. Sediment. Res.* 60, 843–858.
- Waterisotopes.org, 2025. <https://wateriso.utah.edu/waterisotopes/index.html> accessed 2 June 2025.
- Whitcomb, H.A., 1957. A reconnaissance report on the geology and hydrology of the western part of the province of Fezzan, United Kingdom of Libya, no. 57–123, USGS, Washington.
- White, T.D., Asfaw, B., Beyene, Y., Haile-Selassie, Y., Lovejoy, C.O., Suwa, G., WoldeGabriel, G., 2009. *Ardipithecus ramidus* and the paleobiology of early hominids. *Science* 326, 75–86.
- Wu, J., Liu, Z., Stoot, J.B.W., Zhao, Y., Schirone, A., de Lange, G.J., 2017. North-African paleodrainage discharges to the Central Mediterranean during the last 18,000 years: a multiproxy characterization. *Quat. Sci. Rev.* 163, 95–113.
- Xia, Z., Lü, P., Ma, F., Cao, M., Yu, J., 2024. Quantifying dune migration patterns and influencing factors in the Central Sahara Desert. *Catena* 235. <https://doi.org/10.1016/j.catena.2023.107686>.
- Yapp, C.J., 1982. A model for the relationships between precipitation D/H ratios and precipitation intensity. *J. Geophys. Res. Oceans* 87, 9614–9620.
- Zhang, Z., Ramstein, G., Schuster, M., Li, C., Contoux, C., Yan, Q., 2014. Aridification of the Sahara desert caused by Tethys Sea shrinkage during the late Miocene. *Nature* 513, 401–404.
- Zhao, Y., Colin, C., Liu, Z., Paterne, M., Siani, G., Xie, X., 2012. Reconstructing precipitation changes in northeastern Africa during the Quaternary by clay mineralogical and geochemical investigations of Nile deep-sea fan sediments. *Quat. Sci. Rev.* 57, 58–70.
- Zijderveld, J.D.A., 1967. AC demagnetization of rocks: Analysis of results. In: Collinson, D.W., Creer, K.M., Runcorn, S.K. (Eds.), *Methods in Palaeomagnetism, Developments in Solid Earth Geophysics*, vol. 3. Elsevier, pp. 254–286.